

**A CHEMOSTRATIGRAPHIC STUDY OF REGIONAL AND GLOBAL CONTROLS ON
DEPOSITION AND PRESERVATION OF LATE CAMBRIAN SHALES AND
CARBONATES OF THE CONASAUGA GROUP, APPALACHIAN BASIN, USA**

by

Justin Earl Mackey

B.S. Earth Science, Northeastern Illinois University, 2012

Submitted to the Graduate Faculty of the
Dietrich School of Arts and Sciences in partial fulfillment
of the requirements for the degree of
Master of Science in Geology and Environmental Science

University of Pittsburgh

2017

UNIVERSITY OF PITTSBURGH
Dietrich School of Arts and Sciences

This thesis was presented

by

Justin Earl Mackey

It was defended on

March 23rd, 2017

and approved by

Dr. Nadine McQuarrie, Associate Professor, Department of Geology and Environmental
Science

Dr. Rosemary Capo, Associate Professor, Department of Geology and Environmental Science

Thesis Advisor: Dr. Brian Stewart, Associate Professor, Department of Geology and
Environmental Science

Copyright © by Justin Earl Mackey

2017

**A CHEMOSTRATIGRAPHIC STUDY OF REGIONAL AND GLOBAL CONTROLS
ON DEPOSITION AND PRESERVATION OF LATE CAMBRIAN SHALES AND
CARBONATES OF THE CONASAUGA GROUP, APPALACHIAN BASIN, USA**

Justin Earl Mackey, M.S.

University of Pittsburgh, 2017

This study reports data from the Late Cambrian Conasauga Group and overlying Copper Ridge Formation of the Central Appalachian region, eastern U.S.A. Geochemical, macro-, and micro-scale analysis of core material from southeastern Ohio was carried out to constrain the extent of oceanic anoxia and to characterize sediment fluxes on the carbonate platform and continental shelf of Laurentia contemporaneous with the Steptoean Positive Carbon Isotope Excursion (SPICE), a Late Cambrian global marine anoxic event. Carbonate sediments (primarily dolomite) record a positive $\delta^{13}\text{C}_{\text{carb}}$ excursion starting in the middle Nolichucky Formation, reaching its peak (+4.3) at the boundary between the Maynardville and Copper Ridge Formations. Strontium isotope ratios in the dolomitic units are only slightly offset from the expected Cambrian seawater values, suggesting minimal post-diagenetic disturbance of isotopic and trace element systematics. Elemental ratios within the lower Nolichucky Shale facies, including Th/U, Fe_T/Al , and Ce/Ce* anomalies, suggest an anoxic water column contemporaneous with the start of the $\delta^{13}\text{C}_{\text{carb}}$ excursion. Selective leaching of carbonate sediments reveal trends in redox-sensitive trace metals (e.g., U, Ni, V) indicative of regional and global marine anoxia during the peak of the Late Cambrian SPICE event.

TABLE OF CONTENTS

PREFACE.....	IX
1.0 INTRODUCTION.....	1
2.0 GEOLOGIC SETTING.....	5
2.1 PALEOZOIC ROCKS OF THE CENTRAL APPALACHIAN REGION....	5
2.2 THE CONASAUGA GROUP.....	7
3.0 MATERIALS AND METHODS	9
3.1 SAMPLING.....	9
3.2 CARBONATE EXTRACTION.....	12
3.3 X-RAY DIFFRACTION	12
3.4 MAJOR AND TRACE ELEMENTS.....	13
3.5 ¹³C AND ¹⁸O ISOTOPE ANALYSIS OF CARBONATE	13
3.6 ⁸⁷SR / ⁸⁶SR OF CARBONATE LEACHATES.....	14
4.0 RESULTS	15
4.1 LITHOSTRATIGRAPHY	15
4.2 MINERALOGY.....	18
4.3 MAJOR AND TRACE ELEMENTS.....	19
4.4 STABLE ISOTOPES.....	33
4.5 SR ISOTOPE STRATIGRAPHY	35
5.0 DISCUSSION	36
5.1 DIAGENESIS AND GEOCHEMICAL PRESERVATION.....	36
5.1.1 Late Cambrian seawater carbon and strontium signals.....	36

5.1.2	Trace element signatures in carbonate	38
5.2	CARBON ISOTOPE CHEMOSTRATIGRAPHY AND CORRELATION	41
5.3	TRACE ELEMENT CYLCE DISRUPTIONS DUE TO SPICE	43
5.3.1	Evidence of anoxia on Laurentian passive margin?	43
5.3.2	Regional and global oceanic trace element fluctuations during SPICE ...	45
5.3.3	Late Cambrian seawater rare earth element chemistry	48
6.0	CONCLUSION.....	49
7.0	SUMMARY	51
	BIBLIOGRAPHY	52

LIST OF TABLES

Table 1: Petrology and mineralogy of study sample set	17
Table 2: Whole rock major element oxide concentrations	21
Table 3: Whole rock trace element concentrations.....	23
Table 4: Major and trace element geochemistry of carbonate fraction	24
Table 5: Bulk whole rock rare earth element concentrations	27
Table 6: Carbonate hosted rare earth element concentrations	28
Table 7: $\delta^{13}\text{C}$, $\delta^{18}\text{O}$, measured and age corrected $^{87/86}\text{Sr}$ of carbonate	34

LIST OF FIGURES

Figure 1: Paleo-reconstruction of Late Cambrian Earth (494 ma).	2
Figure 2: Late Cambrian Paleogeography and Schematic Cross Section of East Laurentia.	6
Figure 3: Schematic Stratigraphic Section.....	10
Figure 4: Flow diagram for analysis of samples in this study.	11
Figure 5: Photomicrographs of Study Formation.	16
Figure 6: Whole rock major element concentrations.....	22
Figure 7: Concentrations of Fe, Mn, U, Ni, and V in the leached carbonate fraction	26
Figure 8: NASC-normalized rare earth element concentrations.....	29
Figure 9: Plane polarized photomicrographs of sample 0714ARIS5060	29
Figure 10: NASC normalized true Ce/Ce* anomaly.	31
Figure 11: Variations in U and Mn in whole rock and carbonate samples.....	32
Figure 12: $\delta^{13}\text{C}$ and $^{87}\text{Sr}/^{86}\text{Sr}$ isotope values of carbonate fraction	37
Figure 13a-h: Regression analysis of geochemical contaminant signatures.....	40
Figure 14: Fe_T/Al , and Th/U mol and U, Ni, V and ΣREE concentrations	44

PREFACE

This is by far the least read component of a thesis, so I'll keep it short. I would like to thank the American Chemical Society's Petroleum Research Fund for funding my graduate research and the University of Pittsburgh for initial tuition support while I was still finding my "way". I would like to thank my fellow and former lab mates Irene, Monica, Ben, Zach, Matt and Samantha for their support on matters related to both academia and not. Thai, you're the best post-doctoral confidant and advisor a young aspiring geochemist could ask for. And a hero, but we won't talk about that here. Thanks for your intuition and critical questions during my defense, especially the latter. I owe a great deal of gratitude to my committee members Dr. Nadine McQuarrie and Dr. Rosemary Capo for actually reading my thesis and providing sage advice. I sincerely appreciate the tutelage and patience of my thesis advisor, Dr. Brian Stewart. Brian, you're a patient man and for that I am grateful. You helped formulate the questions entertained in this thesis and were somehow able to wrangle me into writing a cohesive scientific body of work while having a baby. Sorry about the oven. I am also thankful for the friendship and comradery from my fellow graduate students in the Department of Geology and Environmental Science. You are all amazing, empathetic people and are going to do great things. Finally, I am most grateful for the love and support from my wife, Sophie. There is no way I could have done this without you.

1.0 INTRODUCTION

The occurrence of black shale in the geologic record is largely associated with euxinic and anoxic depositional environments, which allow significant organic carbon preservation and associated hydrocarbon resources (Berry and Wilde, 1978; Arthur and Sageman, 1994; Ryder et al., 2005; Gill et al., 2011; Gautier et al., 2013). Widespread deposition of black shale facies have been interpreted as global oceanic anoxia events (Arthur and Sageman, 1994; Meyer and Kump, 2008), that resulted in large perturbations in the biogeochemical cycling of nutrients (C,N, P) and redox-sensitive elements (Meyer and Kump, 2008; Lyons et al., 2009; Gill et al., 2011; Ozaki et al., 2011). Here I report data from the Late Cambrian Conasauga group of the Central Appalachian Basin, which has been linked to such a global anoxic event (Glumac and Walker, 1998; Ryder et al., 2005; Meyer and Kump, 2008).

The Conasauga Group is composed of interbedded shale and carbonate sequences deposited on the eastern Laurentian passive margin and known to contain economic hydrocarbon deposits (Hasson and Haase, 1988b; Glumac and Walker, 2000; Ryder et al., 2005). Previous work on this sequence in the Valley and Ridge province of Tennessee revealed evidence of a positive $\delta^{13}\text{C}_{\text{carb}}$ excursion (Glumac and Walker, 1998) contemporaneous with a purported global event known as the Steptoean Positive Carbon Isotope Excursion, or SPICE (Figure 1.) (Brasier, 1993; Saltzman et al., 1998; Saltzman et al., 2000a; Kouchinsky et al., 2008; Ahlberg et al., 2009; Woods et al., 2011; Ng et al., 2014). The SPICE event was rapid and persistent (spanning



Figure 1: Paleo-reconstruction of Late Cambrian Earth (494 ma). The Steptoean Positive Carbon Isotope Excursion resulted in +4-6% increase in $\delta^{13}\text{C}_{\text{carb}}$ recorded in sedimentary rocks deposited on Gondwana (Australia and China), West Laurentia (USA), East Laurentia (USA), Siberia, and Kazakhstan (Brasier, 1993; Saltzman et al., 1998; Saltzman et al., 2000a; Kouchinsky et al., 2008; Ahlberg et al., 2009; Woods et al., 2011; Ng et al., 2014). Approximate location of figure 2 outlined in red. Modified from Scotese (2012).

~4 m.y.). It is associated with a 4-6‰ increase in $\delta^{13}\text{C}_{\text{carb}}$, as well as positive $\delta^{34}\text{S}$ and negative $\delta^{238}\text{U}$ excursions, and is bookended by episodes of biological turnover (Saltzman et al., 1998; Saltzman et al., 2000a; Kouchinsky et al., 2008; Ahlberg et al., 2009; Gill et al., 2011; Woods et al., 2011; Dahl et al., 2014; Gerhardt and Gill, 2016).

The SPICE is attributed to O^2 -depleted bottom waters breaching continental shelves (Gill et al., 2011) as a result of sea-level rise (Osleger and Read, 1993). This led to elevated phosphorus availability in the water column (Dahl et al., 2014) and spurred productivity and enhanced organic carbon (C_{org}) burial (Berry and Wilde, 1978; Saltzman et al., 2000a; Saltzman and Thomas, 2012; Dahl et al., 2014). Anoxia-driven phosphorus availability can only support productivity if there is sufficient trace element (e.g., Mo, Fe, V and Ni) bioavailability and nitrogen fixation to facilitate organic matter generation (Redfield, 1958; Saltzman, 2005). A negative feedback in this model is that anoxia causes denitrification and a drawdown of trace elements from the water column (Algeo, 2004; Saltzman, 2005; Brumsack, 2006). In this study we investigate the distal portion of an organic-rich shale unit (the Nolichucky Formation) and adjacent carbonates on the Laurentian continental shelf to establish a baseline chemostratigraphy of the Late Cambrian Conasauga Group in southeastern Ohio and address the following questions: (1) What was the western (continental-ward) limit of anoxia and euxinia on the eastern Laurentia continental shelf during SPICE? (2) Is there a relationship between the shale facies within the upper Conasauga Group and the increase in marine organic matter deposition? (3) What can the associated carbonate sediments tell us about global changes in the oceanic trace element inventories prior to and during SPICE? The event could have resulted in dramatic increases in atmospheric pO_2 (Saltzman et al., 2011), and concomitant changes in ocean chemistry that have been recorded in Late Cambrian platform carbonates in other parts of the world (Meyer and Kump, 2008; Gill et al., 2011).

A better understanding of the geochemical stratigraphy within the Conasauga Group and Copper Ridge Dolomite (Knox Group) will aid in stratigraphic correlation of upper Cambrian Laurentian sediments within the Central Appalachian region and expand on our knowledge of a Cambrian aged petroleum system currently of interest (Ryder et al., 2005). This study integrates stratigraphy, $\delta^{13}\text{C}_{\text{carb}}$ and $^{87}\text{Sr}/^{86}\text{Sr}$ with trace element data to establish a chemostratigraphy of core material sampling the Upper Cambrian Conasauga Group, in the Central Appalachian region prior to and during SPICE.

2.0 GEOLOGIC SETTING

2.1 PALEOZOIC ROCKS OF THE CENTRAL APPALACHIAN REGION

The samples for this study consist of core material from Southeastern Ohio in the Central Appalachian Basin (Figure 2). The sample interval contain Middle and Late Cambrian sedimentary rocks (~497-493 Ma) deposited off the coast of Laurentia, including the Maryville Limestone, Nolichucky Shale and Maynardville Limestone Formations of the Conasauga group, as well as portions of and the Copper Ridge Formation of the overlying Knox Group. Middle to Late Cambrian sedimentation in the Central Appalachian region was influenced by pre-existing basement structures and sea level fluctuations during the Sauk II supersequence (Osleger and Read, 1993; Read and Repetski, 2012). The main structural control during deposition was a southwest to northeast trending series of steep normal faults known as the Rome Trough. Seismic studies and exploratory wells delineate a northern high wall bounding a basin more than 7,000 m below sea-level (Gao et al., 2000; Harris et al., 2004). Clastic sediments deposited within and adjacent to the trough were likely supplied by the Laurentia craton (Janssens, 1973; Banjade, 2011). Initial faulting started during Early Cambrian rifting and continued through the Middle Cambrian (Thomas, 1991; Read and Repetski, 2012), causing significant shifts in sedimentation within and outside the boundaries of the Rome Trough (Hasson and Haase, 1988a; Harris et al., 2004; Read and Repetski, 2012). Early, Middle and early Late Cambrian

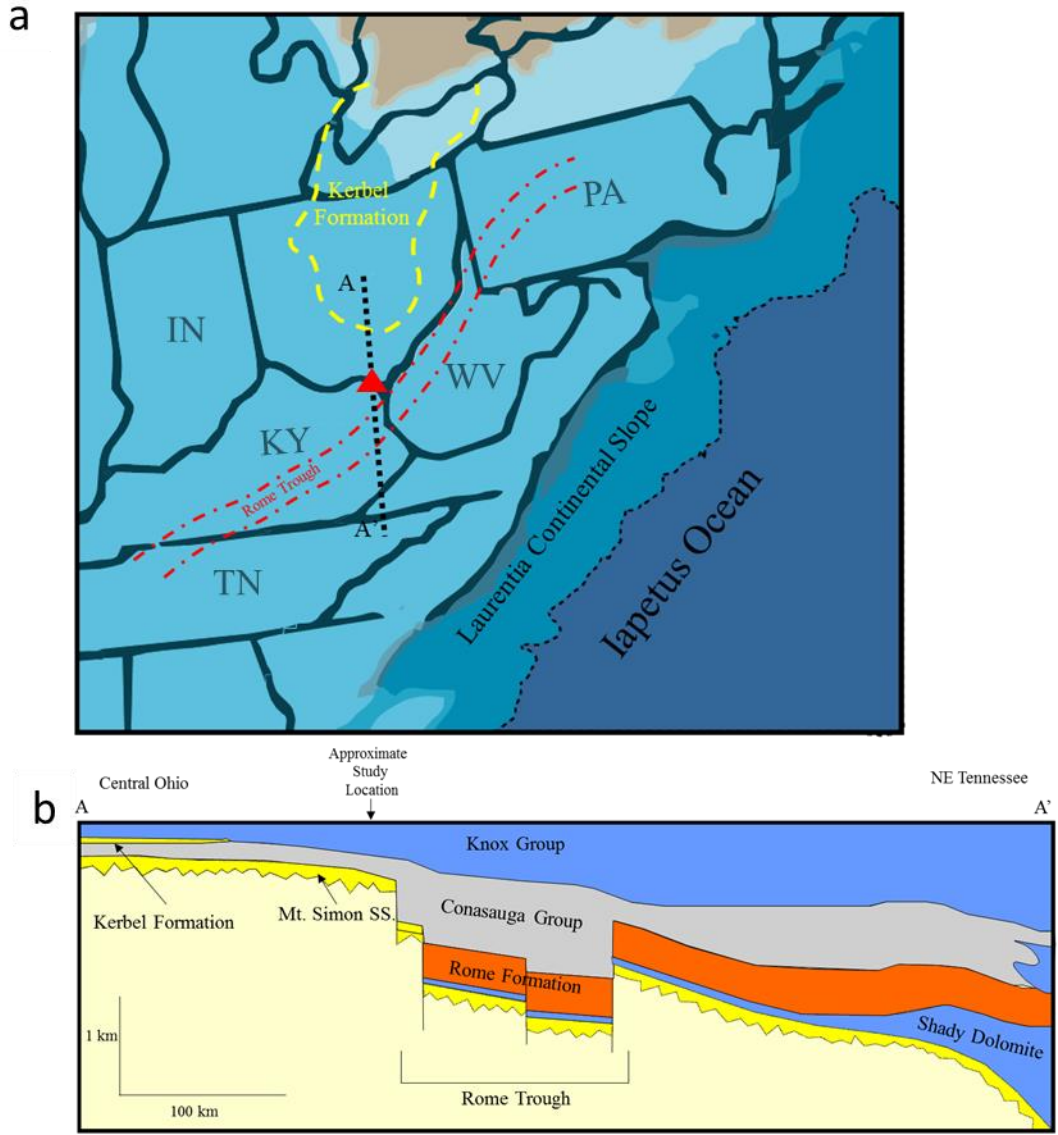


Figure 2: Late Cambrian Paleogeography and Schematic Cross Section of East Laurentia. a) Late Cambrian carbonate platform of Eastern Laurentia with delineation of the Kerbel Formation, the Rome Trough and the study core location (triangle); b) schematic cross section of Paleozoic sedimentation across A-A' (modified from Blakey 2006).

sedimentary rocks thicken southward from the study location into the trough and adjacent depocenters and then transition seaward to outer-shelf/slope marine carbonates (Hasson and Haase, 1988a; Glumac and Walker, 2000; Read and Repetski, 2012). Cratonic influence on sedimentation during the Late Cambrian increases northward from the study location as evidenced by the transition from carbonate-dominated sedimentary rocks at our study site to a clastic-dominated deltaic sedimentary package known as the Kerbel Formation, which extends northward into central Ohio (Figure 2) (Janssens, 1973; Harris et al., 2004). The Late Cambrian and Lower Ordovician Knox Group conformably overlies the carbonate and clastic sequences of the Early to lower Late Cambrian time. The Knox Super-Group represents thick pericratonic successions of carbonate resulting from long periods of stable, shallow passive margin sedimentation (Taylor et al., 2012).

2.2 THE CONASAUGA GROUP

The Conasauga Group is a cyclical package of Middle and Upper Cambrian clastic and carbonate sedimentary rocks deposited on the passive margin of Laurentia. The group represents a prograding carbonate ramp and distal intrashelf basin resulting from episodic transgression and regression (Hasson and Haase, 1988a; Harris et al., 2004). The earliest formations of the group, the Middle Cambrian Pumpkin Valley Shale, Rutledge Limestone and Rogersville Shale Formations, are confined to the Rome Trough. The Middle Cambrian Maryville Formation is an arenaceous limestone occurring both within and outside of the Rome Trough. The formation is thickest within the trough and the adjacent Conasauga intrashelf basin further southward. The limestone grades into the clastic-dominated Eu Claire Formation to the north, toward the Middle

Cambrian Laurentia craton (Ryder et al.; Janssens, 1973; Hasson and Haase, 1988a; Harris et al., 2004). Overlying the Maryville Limestone Formation is the Late Cambrian Nolichucky Formation. The Nolichucky Formation, is a clastic-dominated sequence of grey, purple and black shales and carbonate. The Nolichucky Formation resulted from a eustatic rise in sea-level, flooding the Maryville limestone platform with prodeltaic sediments from Laurentia (Glumac and Walker, 2000; Ettensohn, 2008). The Nolichucky Formation was deposited within and outside of the Rome Trough and has a greater lateral extent than earlier Conasauga Group sedimentary rocks shifts confined to within the Rome Trough (Glumac and Walker, 2000; Harris et al., 2004). The Nolichucky Formation increases in thickness and organic content to south into what is referred to as the Conasauga Intrashelf Basin (Hasson and Haase, 1988b; Glumac and Walker, 2000; Read and Repetski, 2012) where it is a producing hydrocarbon play (Pashin et al., 2012). The formation contains the end-Marjuman trilobite extinction (Glumac and Walker, 1998; Taylor et al., 2012; Gerhardt and Gill, 2016). The youngest unit within the Conasauga Group is the Maynardville Formation. It is composed of a lower subtidal and an upper peritidal facies that marks the shift to Knox-type sedimentation. The contact between the Maynardville Formation and the overlying Copper Ridge Formation coincides with a sea-level lowstand referred to as the Sauk II-III Sub-regression (Saltzman et al., 2004; Read and Repetski, 2012; Taylor et al., 2012).

3.0 MATERIALS AND METHODS

3.1 SAMPLING

A core extracted from an exploratory well located in Scioto county, Ohio (Figure 2) provides a continuous section that contains the Upper Cambrian SPICE interval based on its correlation with other sections in both Eastern and Western Laurentia passive margin sediments (Glumac and Walker, 1998; Saltzman et al., 1998; Glumac and Walker, 2000). Core billets (28 total) were cut at 7.5 m intervals over a 106 m section of core (Fig. 3), avoiding sampling of secondary bedding structures and with denser sampling every 1.5 m near formation boundaries. The exterior of the core billets was cut using a diamond bladed circular saw to remove any possible contaminated material. Chips were cut for petrographic analysis, and the remaining sample pieces were washed in DI water and ethanol. The cleaned billets were then powdered in a tungsten carbide ball mill for 4 minutes to a particle size of <20 microns. Four splits were taken for subsequent analysis. The study methodology is summarized in Figure 4.

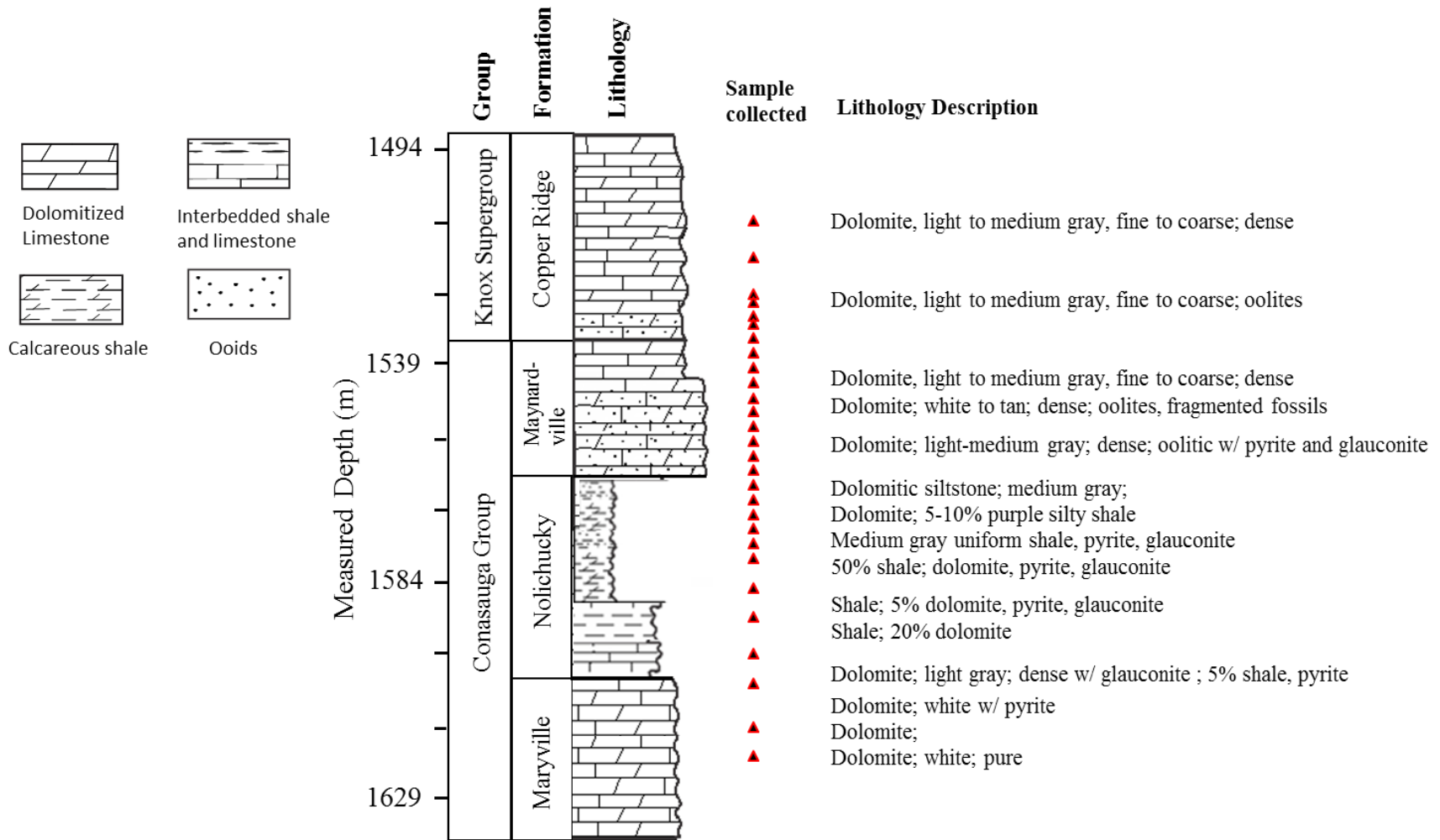


Figure 3: Schematic Stratigraphic Section showing sample locations and core descriptions.

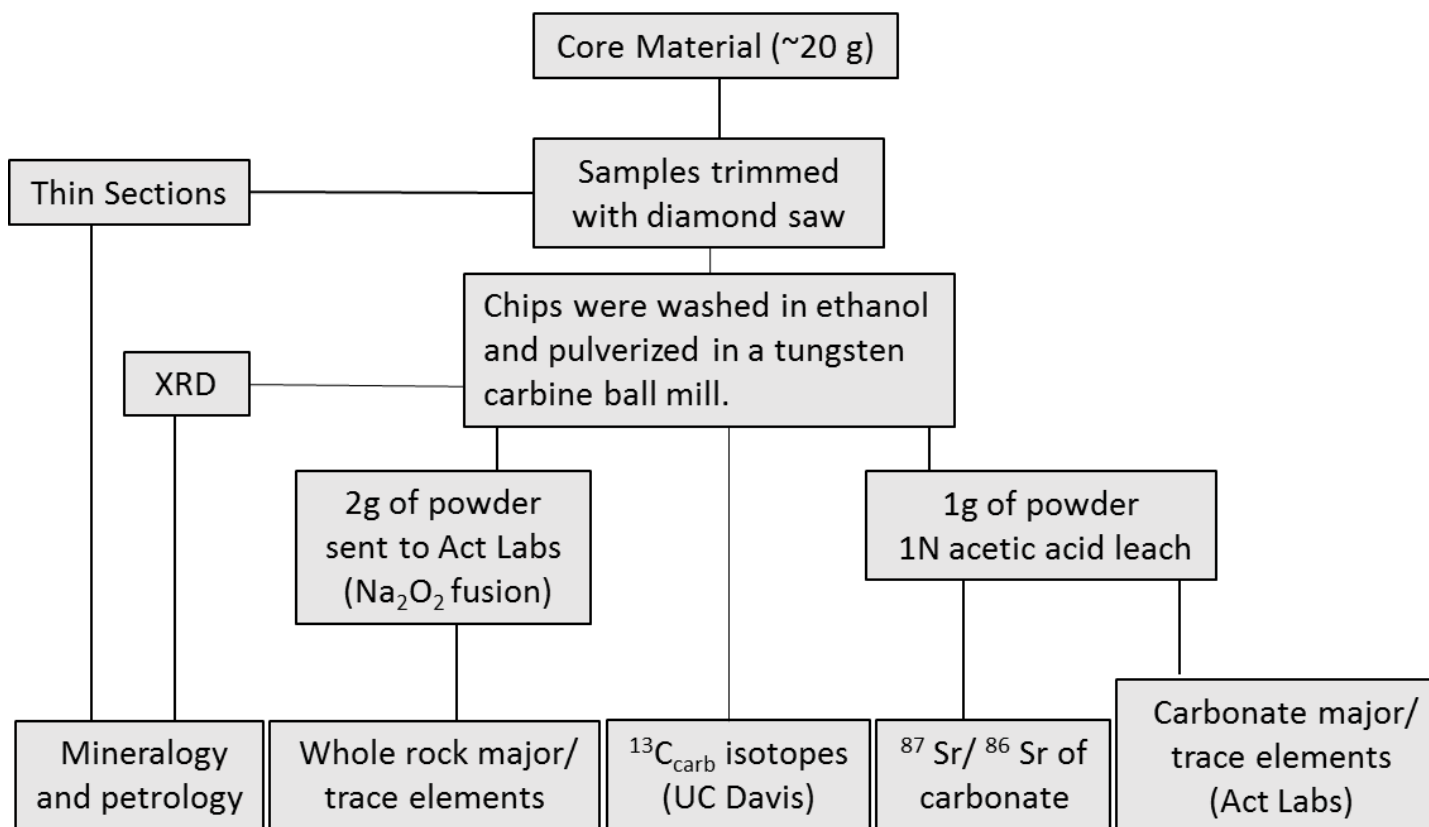


Figure 4: Flow diagram for analysis of samples in this study.

3.2 CARBONATE EXTRACTION

A selective leaching method was used to obtain the carbonate-hosted trace element concentrations (Tissot and Dauphas, 2015). The powdered aliquots were added to a 50 ml polypropylene centrifuge tube and shaken for 24 hours in ultra-pure water at a 40:1 mass ratio to remove water-soluble salts. The H₂O solution was removed via pipette and discarded. An equal amount of 1M glacial acetic acid (HOAc) was added to the centrifuge tubes and samples were shaken for 24 hours, centrifuged, and the leachate was pipetted into acid-washed pre-weighed sample bottles. The HOAc process was then repeated a second time, and the HOAc was added to the same bottles. The leachates were then evaporated in an acid-washed PMP beaker and re-dissolved in 2% Ultrapure HNO₃ for elemental and isotopic analysis. Aliquots were taken from the leachate solution for trace and rare earth element analysis by Activation Laboratories Ltd.

3.3 X-RAY DIFFRACTION

Powdered samples were homogenized with ~10 % by weight ZnO standard, back-loaded into a powder mount, and analyzed on a PANalytical X'Pert Pro diffractometer using Cu K α radiation. The analysis was ran at 40 mA, 45 kV power settings with a 2 $^\circ$ θ step size of 0.05 and step time of 113.73 seconds. Diffraction patterns and d-spacings were interpreted using Highscore Plus

software suite. Mineral quantification was determined using a modification to the mineral intensity factor method of by Środoń et al. (2001).

3.4 MAJOR AND TRACE ELEMENTS

Approximately two grams of sample, sample duplicates and USGS SGR-1b Standard, were analyzed by Activation Laboratories Ltd. Powdered samples were digested using sodium peroxide fusions (precluding Na₂O and LOI analysis) and analyzed by ICP-MS. Duplicate sample values and analysis of certified standards yield less than 6% error margins on major and trace elements.

3.5 ¹³C AND ¹⁸O ISOTOPE ANALYSIS OF CARBONATE

Aliquots of powdered, bulk carbonate samples were analyzed at the University of California, Davis Stable Isotope Laboratory for δ¹³C and δ¹⁸O isotopic composition. Samples were roasted at 375°C for 30 min in vacuo, then reacted in supersaturated H₃PO₄ (sp. gr. 1.93) at 90°C using an Isocarb common acid bath autocarbonate device. Reaction time was increased from 12 to 20 minutes to ensure total carbonate reaction of dolomitic samples. The resulting CO₂ was analyzed by a Micromass Optima isotope ratio mass spectrometer (IRMS). Oxygen and carbon isotope values are reported in ‰ notation relative to the V-PDB (Vienna Pee Dee Belemnite) standard where:

$$\delta^{18}\text{O (or } \delta^{13}\text{C)} = [({}^{18}\text{O}/{}^{16}\text{O sample} / {}^{18}\text{O}/{}^{16}\text{O standard}) - 1] \times 1000$$

The analytical precision for these samples is $\pm 0.047\%$ and $\pm 0.038\%$ for $\delta^{18}\text{O}$ and $\delta^{13}\text{C}$ respectively ($\pm 1\text{s}$), based on repeat analyses of a laboratory calcite standard that was previously calibrated to NBS-19.

3.6 $^{87}\text{Sr} / ^{86}\text{Sr}$ OF CARBONATE LEACHATES

All strontium prep was performed in a clean lab under a HEPA filtered hood. Aliquots of the leachate containing 2 μg of Sr in HNO_3 were dried in a Teflon beaker at 100°C . The samples were re-suspended in 250 μL of ultra-pure 8N HNO_3 and processed through microcolumns containing 300 μL Sr-Resin®, following the procedure of Wall et al. (2013). Samples were analyzed on Thermo Scientific Neptune Plus double-focusing MC-ICP-MS at the University of Pittsburgh.

4.0 RESULTS

4.1 LITHOSTRATIGRAPHY

The core samples reported here (Figure 3) consist of bulk siliciclastic and carbonate rocks deposited on the Eastern Shelf of Laurentia during the Middle to Late Cambrian (~497-494 Ma) and represents shallowing from a subtidal to a peritidal and supratidal depositional environments. Photomicrographs of the major stratigraphic units are shown in Figure 5. The majority of primary calcite has been replaced by dolomite during burial diagenesis. The Nolichucky, Maynardville Formations, and Copper Ridge Formations contain authigenic microcline (Table 1), likely as a result of potassium-rich brine migration during the Allegheny Orogeny (Hearn and Sutter, 1985a).

The base of the study interval (1685-1591 m) is a dolomitized dismicrite of the Maryville Formation (Figure 5e). Gamma log correlation (not shown) shows a sharp increase in gamma A.P.I. at the contact between the Maryville and Nolichucky Formations (Harris et al., 2004). This likely reflects a petrologic transition from the Maryville Formation carbonate to the sand- and carbonate-dominated lower facies of the Nolichucky Formation. This consists of 46 meters of interbedded intraclastic carbonate and siliciclastic rocks with a basal intramicrite containing sub-angular, moderately sorted quartz grains in a fine grained carbonate matrix. At 1579 m this transitions to a clay-dominated glauconitic intrasparite with micrite intraclasts (Figure 5h).

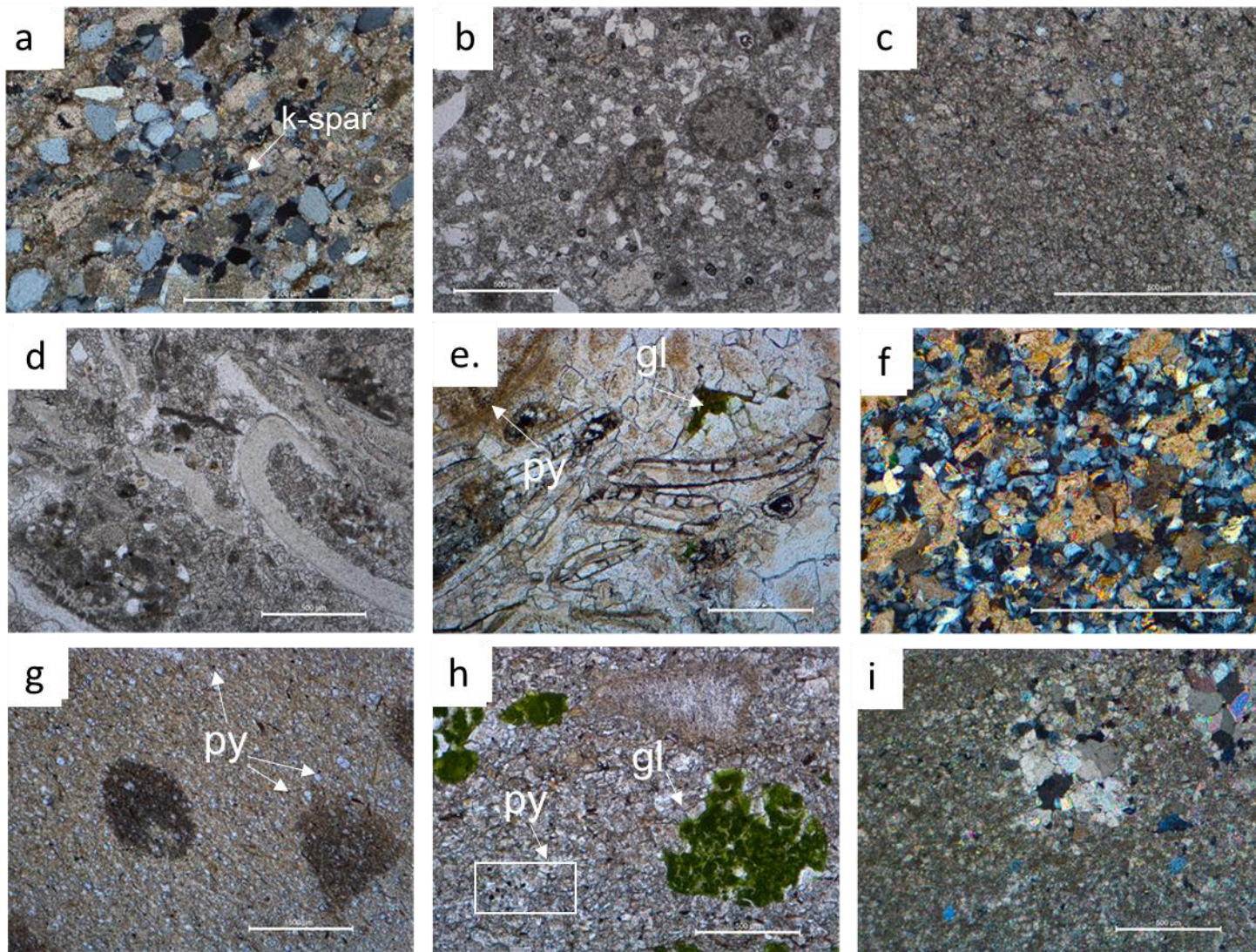


Figure 5: Photomicrographs of Study Formation. a,b) Copper Ridge Formation, c) Maynardville Formation peritidal dismicrite, d) Maynardville Formation peritidal oolitic biomicrite, e) Maynardville Formation subtidal unsorted biosparite, f) Nolichucky Formation intrasparite, g) Nolichucky Formation intrasparite, h) Nolichucky Formation intrasparite, i) Maryville Formation dismicrite.

Table 1: Petrology and mineralogy of study sample set. Semi-quantitative mineralogy was determined by XRD except where noted.

Sample ID	Formation	Quartz	Clay	Dolomite	Calcite	K-Feldspar	Pyrite*	Glauconite*	Folk Classification
0715ARIS 4925	Copper Ridge Dolomite	X		X					Intrasparite
0715ARIS 4950	Copper Ridge Dolomite	X		X		x			intrasparite
0715ARIS 4965	Copper Ridge Dolomite	X		X		x			
0715ARIS 4980	Maynardville Limestone	X		X		x			Dismicrite
0715ARIS 5000	Maynardville Limestone	X		X		x			Dismicrite
0715ARIS 5021	Maynardville Limestone	X		X	X	x			Oolitic biomicrite
0715ARIS 5040	Maynardville Limestone	X		X		X			Laminated intramicrite
0715ARIS 5060	Maynardville Limestone						x		Unsorted biosparite
0715ARIS 5080	Nolichucky Shale	X	x	X		x			Intrasparite
0715ARIS 5100	Nolichucky Shale						x	x	Intrasparite
0715ARIS 5110	Nolichucky Shale	X	X						
0715ARIS 5120	Nolichucky Shale	X	x	X	X	x	x	x	Intrasparite
ARIS5150	Nolichucky Shale	X	X	x	x		x	x	Intrasparite
ARIS5170	Nolichucky Shale						x		Intrasparite
ARIS5195	Nolichucky Shale			X					
ARIS5215	Maryville Limestone	X		X			x		Intramicrite
ARIS5245	Maryville Limestone	X		X					
ARIS5265	Maryville Limestone	X		X					Dismicrite

X Denotes major mineral constituent.

x Denotes Minor mineral constituent.

*Detected in thin section.

Samples in this interval consist of relatively well sorted, sub-angular quartz grains that are grain supported. Interstitial pyrite is present in trace amounts, and the sediments have dolomitic carbonate cement. Clay content starts to decrease at approximately 1554 m and the lithology transitions to a sandy-siltstone with small, sub-meter-scale lenses of limestone to the top of the section. The Nolichucky Formation is not a homogenous shale unit at this location. Clastic particle sizes range in size from clay to sand, and the unit contains an appreciable amount of carbonate both as primary carbonate and as matrix cement.

At 1548 m the overlying Maynardville Formation marks a transition from siliciclastic to carbonate dominated sedimentation. The base of the formation (1548 m) consists of peloidal biosparite. The sediments are a poorly sorted, sub-horizontally bedded mix of trilobite and echinoderm fossils with fragments of micrite interclasts that indicate a moderately agitated shallow subtidal environment. At approximately 1536 m the lithology shifts to a laminated intramicrite, then at 1530 meters depth to an oolitic biosparite with abundant brachiopod and trilobite fragments and ooid packstone laminae, likely indicative of a high energy shallow ooid shoal. It is capped with a dismicrite and marks the transition from subtidal to intertidal depositional environment.

The top of the study interval (1494-1509 m) contains the Copper Ridge Formation, a lower subdivision of the Knox Group. In our section it (Figure 5a-b) is a poorly sorted intrasparite predominately composed of quartz, calcite, dolomite and authigenic feldspar.

4.2 MINERALOGY

XRD results are summarized in Table 1. The presumed protolith limestone was partially or completely replaced by dolomite. X-ray diffraction reveals minor amounts of microcline in the

Nolichucky, Maynardville and Copper Ridge Formations. However, only the Copper Ridge Dolomite contained visible subhedral microcline in thin section (Fig. 5a). It is likely that the larger microcline is of detrital origin, being visible only in the lowstand (Sauk II-III sub-regression) sediments. Other feldspars detected by XRD are more likely of authigenic origin and contemporaneous to those found in other mid-continent Cambro-Ordovician carbonate sediments associated with a potassium metasomatic event during the Permian (Hearn and Sutter, 1985b). The Maryville Formation consists of fine grained dolomite and lenses of sparry dolomite in birds-eye structures (Figure 5i). At approximately 1590 m, the formation contains cross-cutting pyrite-hosting carbonate veins (not shown). The lower Nolichucky Formation (not shown) is composed of dolomite and detrital quartz. At approximately 1575 m (Figure 5h) the clay content increases significantly, with minor amounts of glauconite in the shale-rich facies. Small, cubic opaque minerals, likely pyrite, can be seen in thin section (Figure 5g-h). Clay content generally decreases as up section to ~1560 m. The upper Nolichucky Formation is composed of generally well sorted quartz grains and dolomitic cement (Figure 5f). The Maynardville Formation is composed of calcite and dolomite with increasing quartz content up section, with the exception of a calcite dominant fossiliferous zone at 1530 m (Figure 5d).

4.3 MAJOR AND TRACE ELEMENTS

Whole rock major element oxide percentages are summarized in Table 2. SiO_2 and Al_2O_3 concentrations are highest in the Nolichucky samples and in general decrease through the Maynardville Formation and with a slight increase in in the Copper Ridge Formation (Figure 6). MgO and CaO are highest in the Maryville Formation and within the carbonate facies of the other

units. MgO/CaO ratios are consistent with stoichiometric dolomite with the exception of higher Mg and Al content in the clastic-rich dolomite cemented facies of the Nolichucky Formation (~1570 m) and a lower MgO/CaO at ~1550m, within the Maynardville. The increased Mg and Al content within the Nolichucky Formation is due to the presence of Mg-rich aluminosilicates, whereas the decrease is likely associated with calcite in primary fossil assemblages. Al₂O₃ increases from 1585 m within the lower Nolichucky Formation to and then begins to decrease at ~ 1570 m. SiO₂ increases coeval to the start of Nolichucky Formation deposition to ~1554 meters depth and decreases at the contact between the carbonate dominated Maynardville Formation.

Whole rock trace element data are summarized in Table 3. Trace metals, U, Fe, Cu and V are highest within the clastic facies of the Nolichucky Formation and subtidal Maynardville Formation facies. Mn concentrations are elevated in the carbonate facies within and below the subtidal Maynardville Formation facies. The lowest Mn value is within Nolichucky Formation at ~1554 m depth.

Carbonate geochemistry (based on acetic acid leaches) is summarized in Table 4. The carbonate portions contain significant concentrations of Mn (353-3470 mg kg⁻¹) and Fe (1.9- 43.6 mg kg⁻¹). Al and Si concentrations are highest (2820 and 5210 mg kg⁻¹ respectively) in the shale facies of the Nolichucky Formation. Si and Al concentrations this high within carbonate

Table 2: Whole rock major element oxide concentrations in percent for the sample interval. Note data is missing Na values and LOI due to Na₂O₂fusion. Samples were analyzed on ICP-MS

Depth (m)	Sample ID	SiO ₂	TiO ₂	Al ₂ O ₃	FeO	CaO	MgO	K ₂ O	S
		-----%							
1501	0715ARIS 4925	11.6	0.03	1.2	0.31	19.7	11.9	1.08	0.23
1509	0715ARIS 4950	26.1	0.23	4.3	0.59	15.6	8.92	3.85	0.35
1513	0715ARIS 4965	24.8	0.20	4.2	0.77	15.9	8.97	3.61	0.54
1518	0715ARIS 4980	12.0	0.13	2.6	0.72	19	10.9	2.17	0.24
1524	0715ARIS 5000	12.2	0.13	2.9	1.03	19.2	10.8	2.17	0.17
1530	0715ARIS 5021	27.4	0.30	6.4	1.70	21.8	2.56	4.46	0.36
1536	0715ARIS 5040	21.2	0.22	4.6	2.59	17.4	7.77	3.37	0.37
1542	0715ARIS 5060	3.9	0.03	0.9	3.69	22.8	9.64	0.72	0.64
1548	0715ARIS 5080	59.5	0.35	7.6	2.24	6.42	3.27	6.26	0.45
1554	0715ARIS 5100	*	0.62	12.0	3.73	1.36	1.25	9.03	0.03
1561	0715ARIS 5120	55.2	0.72	17.8	4.71	1.94	1.97	11.93	0.32
1570	ARIS5150	34.9	0.45	9.6	3.37	10.5	6.01	6.99	0.27
1576	ARIS5170	18.3	0.18	3.3	3.05	16.7	9.62	2.77	0.13
1583	ARIS5195	2.1		0.3	0.75	21.8	12.9	0.24	
1590	ARIS5215	10.2	0.05	2.0	0.64	19.7	11.7	1.81	0.09
1599	ARIS5245	4.5	0.07	1.3	0.76	20.9	12.6	0.96	0.11
1605	ARIS5265	2.5		0.4	0.30	21.7	13.3	0.24	0.05

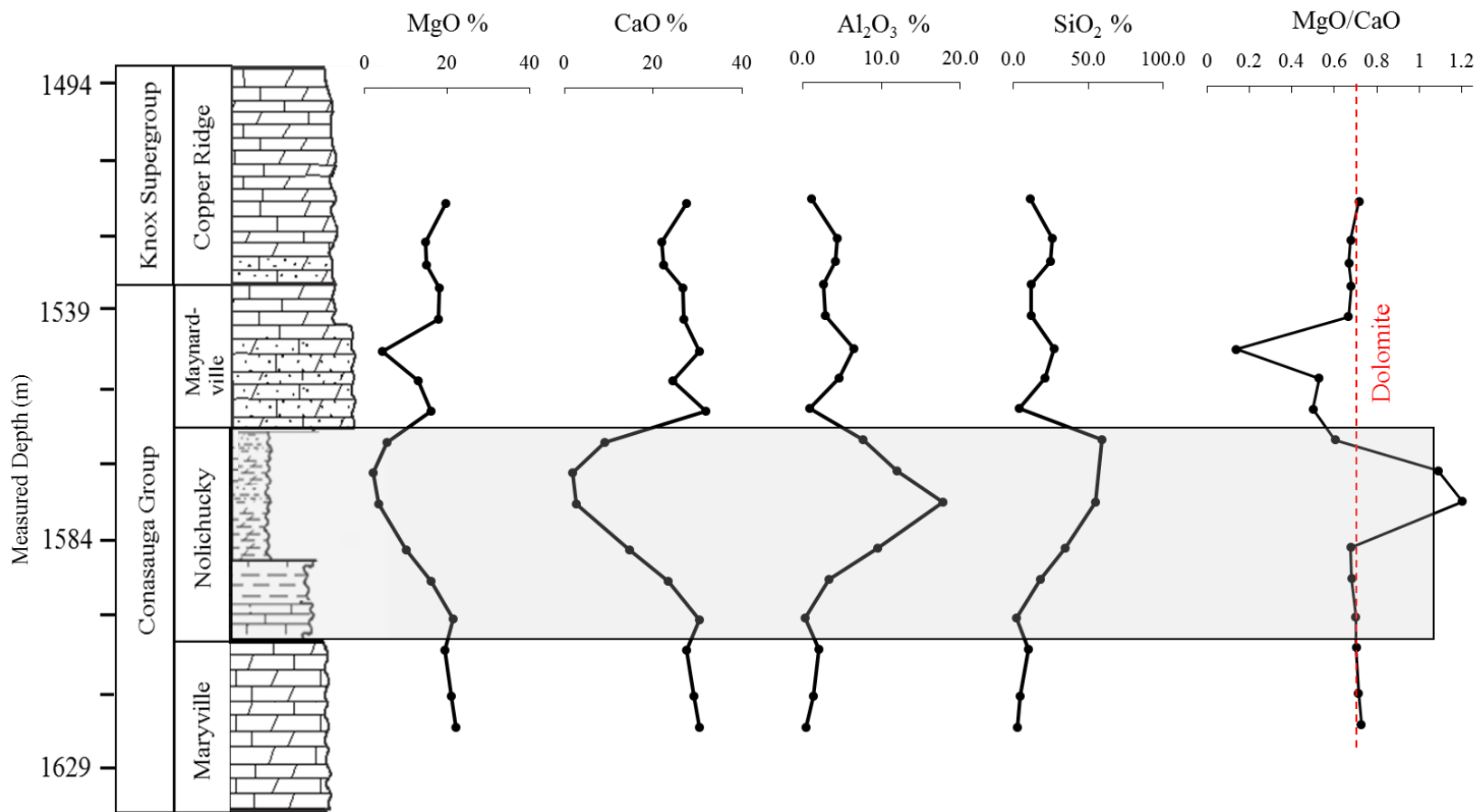


Figure 6: Whole rock major element concentrations (wt%) for samples in this study.

Table 3: Whole rock trace element concentrations (mg/kg) of bulk powdered samples were measured by ICP-MS. Note data is missing LOI due to Na₂O₂fusion.

Depth (m)	Sample ID	B	Ba	Co	Cr	Cu	Ga	Mn	Ni	Pb	Rb	Se	Sn	Sr	Th	Tl	U	V	W	Y
		-----mg kg ⁻¹ -----																		
1501	0715ARIS 4925	40	112	3.3	40	*	1.1	250	20	13.6	9.4	2.3	33.7	80	0.4	1.6	0.3	*	25.8	3.8
1509	0715ARIS 4950	70	339	4.7	70	12	4.6	292	20	42.6	33.5	3.7	42.3	106	2.4	1	1.4	11	24.6	10.9
1513	0715ARIS 4965	40	306	4.6	50	*	4.3	252	20	28.4	31.6	4.7	31	84	2.5	0.4	1.6	14	34.8	10
1518	0715ARIS 4980	50	114	4	40	7	3.1	267	20	16.5	18.8	3	15.3	70	1.8	0.4	1.1	10	26.6	5.3
1524	0715ARIS 5000	60	94	10.2	40	40	3.4	314	20	24.9	23.9	3	13.5	75	1.7	0.3	0.7	9	28.4	6.6
1530	0715ARIS 5021	90	237	7.5	60	24	8	303	30	192	57.7	5.3	9.4	278	4.1	0.5	1.1	29	8.1	10.2
1536	0715ARIS 5040	60	159	7.7	100	105	5.8	834	20	539	37.3	8.7	13.8	151	2.8	0.3	0.9	22	11.3	8.8
1542	0715ARIS 5060	30	29	30.7	40	9	1.7	1980	30	627	7.3	2.2	6	103	3.4	0.7	0.4	*	19.3	25.9
1548	0715ARIS 5080	30	574	9.5	60	89	5.5	740	20	25.6	65.1	2.9	1.7	85	4.6	0.3	1.9	19	75.7	22.2
1554	0715ARIS 5100	60	791	21.9	90	143	12.4	170	30	24.8	88.8	2	19.4	141	10	0.4	2.2	42	174	25.6
1561	0715ARIS 5120	420	417	18.8	130	40	22	348	50	18	166	2.1	81	87	12.6	0.6	2	61	6.2	18.8
1570	ARIS5150	130	358	20.5	80	41	11.3	712	70	21.2	89.1	3.4	37.5	83	7	0.4	1.8	33	25.4	17.9
1576	ARIS5170	70	223	10.9	40	34	6.2	581	60	8.5	39.4	1.8	58.5	77	2.7	0.3	1.4	*	25.7	12.6
1583	ARIS5195	10	20	2.7	30	7	0.6	532	10	*	3.3	2.3	21.9	49	0.1	1.4	0.8	*	12.2	3.8
1590	ARIS5215	*	166	2.4	*	10	1.4	663	20	2.1	15.9	2	3.4	62	0.4	238	1.4	*	19.9	2.6
1599	ARIS5245	30	44	3.4	30	48	1.9	570	20	6.3	11.3	2	*	65	1.5	0.3	1.3	7	12.3	3.8
1605	ARIS5265	*	55	4.3	*	14	0.5	306	20	3.7	3.2	2.2	2.6	55	*	0.7	0.7	*	27.1	1.6

Table 4: Major and trace element geochemistry of carbonate fraction derived from 1N acetic acid leach. All analytes were measured by ICP-MS

Depth (m)	Sample ID	Ca	Mg	Fe	(Ca/Mg) _{Mol}	Si	Ti	Al	Mn	K	Na	As	Ba	Be	Co	Cr	Cs	Cu	Ga
		-----g/kg-----				-----mg kg ⁻¹ -----													
1501	0715ARIS 4925	229	123	1.9	1.1		6.2	71.2	353.6	50.1	95.7	0.4	5.5	0.1	5.1	3.1	0.001		0.8
1509	0715ARIS 4950	232	121	3.3	1.1		3.0	184.0	492.0	169.2	144.1	0.9	7.9	0.2	5.9	11.8	0.001	2.0	2.0
1518	0715ARIS 4980	232	122	4.2	1.1	281.3	4.9	335.3	366.8	297.0	186.8	0.7	8.1	0.3	5.4	6.4	0.003	1.9	1.4
1530	0715ARIS 5021	378	16	2.1	13.8		8.2	307.7	398.5	954.4	233.6	1.1	13.3	0.3	4.1	2.2	0.035	2.0	3.4
1536	0715ARIS 5040	257	103	19.1	1.5	720.1	4.7	531.7	1462.3	913.9	242.6	1.2	21.7	0.8	6.2	5.5	0.006	5.4	3.0
1548	0715ARIS 5080	252	107	43.5	1.4		5.2	1414.8	3471.5	2318.7	589.5	3.0	419.2	0.5	41.3	21.7	0.018	12.5	6.0
1561	0715ARIS 5120	264	98	43.6	1.6	2822.9	5.5	5207.7	3439.3	24659.4	3488.0	4.1	34.6	3.2	84.4	28.9	0.276	31.8	10.3
1570	ARIS 5150	244	113	29.2	1.3	658.2	8.5	1451.2	1926.4	2568.5	359.6	1.8	23.6	0.8	23.9	12.0	0.026	1.5	5.0
1590	ARIS 5215	232	122	6.0	1.1		5.1	124.4	1066.7	117.0	64.3	0.3	5.1	0.1	3.3	1.5	0.003	0.6	0.6
1599	ARIS 5245	231	122	4.4	1.1		7.1	269.3	760.2	194.6	93.6	0.4	11.8		2.8	2.1	0.008	6.8	0.8

Depth (m)	Sample ID	Ga	Ge	Hf	In	Li	Ni	Pb	Rb	Sc	Se	Sr	Th	Tl	U	V	W	Y	Zn	Zr
		-----mg kg ⁻¹ -----																		
1501	0715ARIS 4925	0.8	0.1	0.003	0.005	1.4	0.2	2.6	0.1	1.05	0.7	61.2	0.1	0.0	0.03	7.4	1.1	4.1	1.9	
1509	0715ARIS 4950	2.0	0.2	0.006	0.017	1.5	0.9	4.5	0.2	4.69	1.7	74.6	0.3	0.0	0.1	18.1	0.3	10.3	3.0	
1518	0715ARIS 4980	1.4	0.2	0.005	0.012	1.7	2.9	5.4	0.5	3.26	0.8	63.9	0.5	0.0	0.1	15.3	0.4	5.8	9.1	0.02
1530	0715ARIS 5021	3.4	0.3	0.006	0.015	4.0	3.3	4.3	2.7	4.12	1.7	535.2	0.7	0.0	0.3	3.0	0.1	9.2	2.7	0.03
1536	0715ARIS 5040	3.0	0.3	0.006	0.021	3.7	5.4	4.5	2.3	5.32	1.6	245.9	1.3	0.0	0.3	12.5	0.1	10.9	11.6	0.03
1548	0715ARIS 5080	6.0	0.9	0.028	0.275	2.5	10.7	2.9	3.5	23.19	7.0	148.0	1.7	0.0	0.3	32.2	2.5	36.3	57.9	0.74
1561	0715ARIS 5120	10.3	1.4	0.048	0.226	20.9	52.6	5.5	42.0	51.91	10.6	593.8	8.1	0.1	1.4	20.3	0.1	58.7	32.0	0.21
1570	ARIS 5150	5.0	0.6	0.016	0.070	3.4	11.2	1.9	5.5	13.00	3.9	123.3	3.2	0.0	0.3	17.5	0.5	25.4	14.1	0.07
1590	ARIS 5215	0.6	0.1	0.002	0.004		0.5	0.5	0.4	1.22	0.4	46.7	0.3	0.0	0.5	5.5	0.9	2.9	6.3	0.02
1599	ARIS 5245	0.8	0.1	0.003	0.004		1.1	1.3	1.0		0.69	54.3	0.3	0.0	0.4	6.1	0.3	3.6	6.2	0.02

leaches could indicate partial (~0.5%) leaching of aluminosilicates during the selective acetic acid leach. In the Maryville and Copper Ridge Formations, molar Ca/Mg ratios of the carbonate leaches (~1.1) are within the range of stoichiometric dolomite. The ratios are elevated within the Nolichucky Formation (1.3-1.6) and highest (13.8) within a fossiliferous section within the upper Maynardville Formation. Trace metals U, Fe, V and Ni are highest within the Nolichucky Formation and decrease to the lowest concentrations in the Copper Ridge Formation (Figure 7).

Whole rock and carbonate rare earth element (REE) concentrations are summarized in Tables 5 and 6 respectively. Whole rock and carbonate concentrations normalized to the North American Shale Composite (NASC) (Gromet et al., 1984) are plotted in Figure 8. Whole rock rare earth elements of the clastic-rich Nolichucky Formation plot near NASC values (Fig. 8a). The carbonate facies whole rock samples plot below NASC values, with the exception of one sample within the subtidal Maynardville Formation, which is also enriched in light and middle REE. All samples exhibit a slightly depletion in heavy rare earth elements (HREE). Rare earth element concentrations in carbonate extracted from the Nolichucky Formation are equal to or higher than those of NASC and have elevated MREE concentrations (Fig. 8b). Samples of limestone and dolomite from the Maryville, Maynardville and Copper Ridge Formations have similar patterns and concentrations as the whole rock samples, with the exception of sample 0715ARIS5060 taken at the base of the Maynardville Formation. This is a carbonate sample with the highest Σ REE concentration of all whole rock samples (Figure 8a); however, Σ REE and NASC-normalized plots of the leached carbonate fraction is similar to the other carbonate units. The sample also contains the highest Mn, S, and Pb whole-rock concentrations. A possible explanation for the anomalously high values in this sample is that it contains Mn-oxide coated intraclasts (Figure 9) that were reworked into oxygen-depleted sediments. This would have

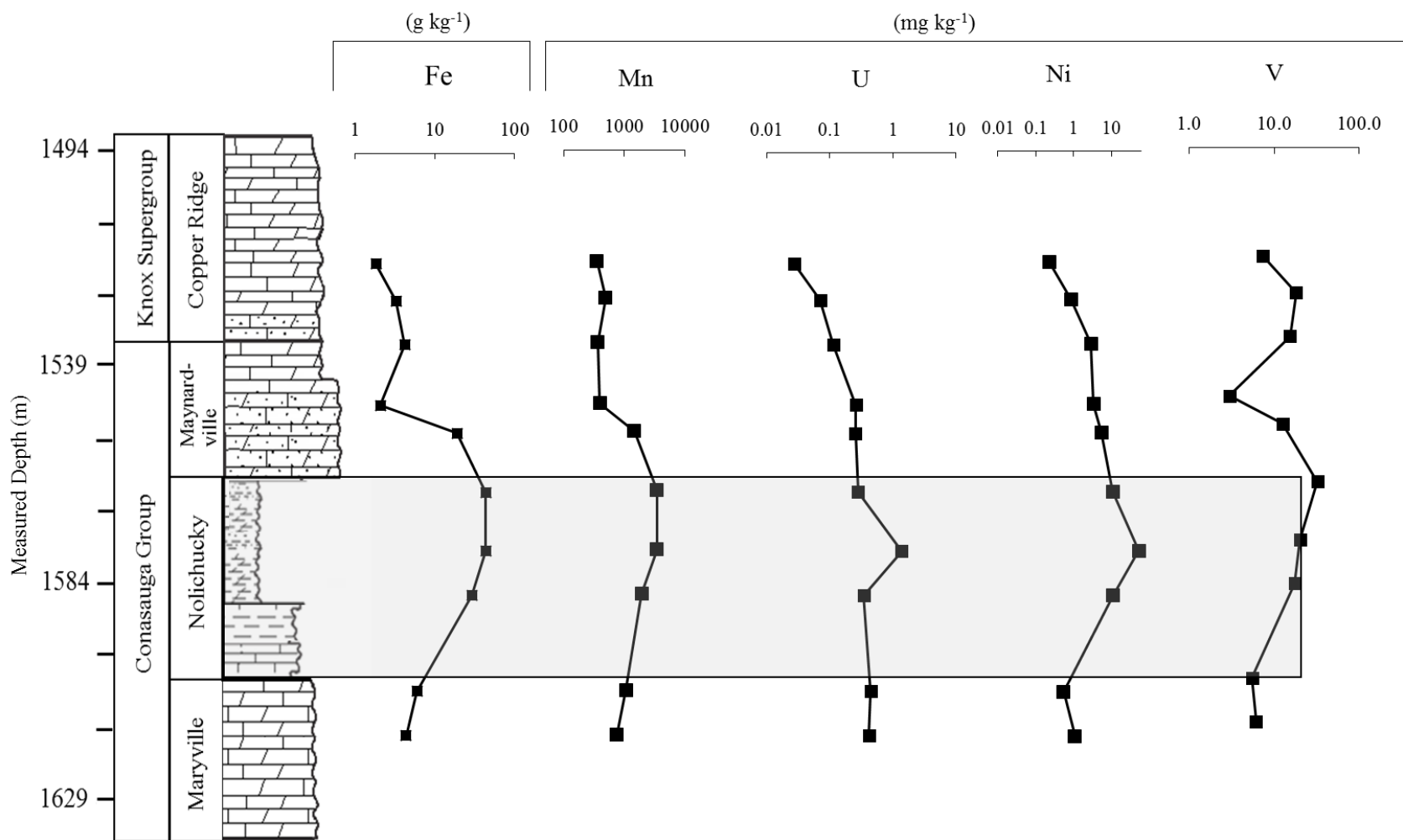


Figure 7: Concentrations of Fe, Mn, U, Ni, and V in the leached carbonate fraction. Note that concentrations are plotted on a logarithmic scale.

Table 5: Bulk whole rock rare earth element concentrations (mg/kg). All analytes measured on ICP-MS.

Depth (m)	Sample ID	La	Ce	Pr	Nd	Sm	Eu	Gd	Tb	Dy	Ho	Er	Tm	Yb
		-----mg kg ⁻¹ -----												
1501	0715ARIS 4925	3.50	10.30	1.00	4.20	0.80	0.20	0.40	*	0.60	*	0.40		0.30
1509	0715ARIS 4950	10.50	28.80	2.90	12.30	2.30	0.50	2.00	0.30	1.90	0.40	1.30	0.20	1.20
1513	0715ARIS 4965	11.00	29.50	3.00	12.60	2.30	0.50	2.00	0.30	1.70	0.30	1.10	0.10	0.90
1518	0715ARIS 4980	7.30	17.40	1.70	6.90	1.20	0.20	0.80	0.10	0.90	*	0.50	*	0.40
1524	0715ARIS 5000	8.70	20.60	2.10	8.20	1.40	0.30	1.10	0.10	1.00	0.20	0.60	*	0.40
1530	0715ARIS 5021	16.70	38.20	4.00	15.40	2.50	0.60	2.00	0.30	1.70	0.40	1.10	0.10	0.90
1536	0715ARIS 5040	15.00	31.60	3.30	12.50	2.10	0.50	1.60	0.20	1.40	0.30	0.90	0.10	0.70
1542	0715ARIS 5060	54.30	130.00	13.10	52.30	8.40	2.10	8.20	0.90	4.50	0.90	2.20	0.30	1.30
1548	0715ARIS 5080	13.90	41.60	5.00	24.00	5.40	1.40	6.00	0.80	4.10	0.80	2.30	0.30	1.80
1554	0715ARIS 5100	27.60	76.40	8.00	35.60	5.60	1.20	5.40	0.80	4.20	0.90	2.70	0.40	2.50
1561	0715ARIS 5120	48.80	98.80	10.40	37.80	5.60	1.20	4.30	0.60	3.20	0.70	2.00	0.30	1.80
1570	ARIS5150	29.30	66.40	7.10	27.60	4.50	1.00	3.80	0.60	3.10	0.70	1.90	0.30	1.60
1576	ARIS5170	12.40	29.50	3.00	11.90	2.20	0.50	2.10	0.30	1.80	0.40	1.20	0.20	1.00
1583	ARIS5195	2.20	5.50	0.50	2.10	0.40	*	0.20	*	0.50	*	0.30	*	0.20
1590	ARIS5215	2.90	7.10	0.70	2.90	0.40	0.10	0.10	*	0.40	*	0.20	*	0.20
1599	ARIS5245	5.10	10.00	1.00	4.00	0.60	0.10	0.30	*	0.50	*	0.30	*	0.30
1605	ARIS5265	2.10	4.40	0.40	1.80	0.30	*	*	*	*	*	0.10	*	*

*Denotes values at or below the detection limit.

Table 6: Carbonate hosted rare earth element concentrations (mg/kg). Concentrations were derived from a selective 1N acetic acid leach. All analytes measured on ICP-MS.

Depth (m)	Sample ID	La	Ce	Pr	Nd	Sm	Eu	Gd	Tb	Dy	Ho	Er	Tm	Yb	Lu
		-----mg kg ⁻¹ -----													
1501	0715ARIS 4925	3.35	9.34	1.02	4.46	0.97	0.23	0.87	0.14	0.84	0.15	0.46	0.06	0.44	0.06
1509	0715ARIS 4950	7.60	20.39	2.40	10.85	2.41	0.58	2.17	0.34	2.00	0.36	1.05	0.14	0.91	0.12
1518	0715ARIS 4980	6.83	15.64	1.77	7.29	1.44	0.32	1.28	0.19	1.09	0.19	0.54	0.06	0.43	0.05
1530	0715ARIS 5021	15.80	32.83	4.33	14.81	2.96	0.59	2.34	0.32	1.70	0.30	0.83	0.10	0.67	0.09
1536	0715ARIS 5040	17.17	32.46	3.87	15.40	2.85	0.59	2.45	0.35	1.95	0.34	0.96	0.11	0.73	0.09
1548	0715ARIS 5080	13.76	54.37	7.87	40.35	10.62	2.61	9.94	1.53	8.33	1.40	3.72	0.43	2.79	0.49
1561	0715ARIS 5120	27.09	103.50	12.35	69.76	15.59	3.59	14.65	2.17	11.92	2.01	5.47	0.64	4.07	0.54
1570	ARIS 5150	14.64	49.44	6.20	28.58	6.24	1.33	5.46	0.85	4.99	0.90	2.63	0.34	2.26	0.31
1590	ARIS 5215	3.02	6.88	0.77	3.27	0.63	0.14	0.57	0.08	0.47	0.09	0.25	0.03	0.21	0.02
1599	ARIS 5245	3.73	8.13	0.93	3.92	0.74	0.16	0.71	0.10	0.59	0.11	0.31	0.04	0.25	0.03

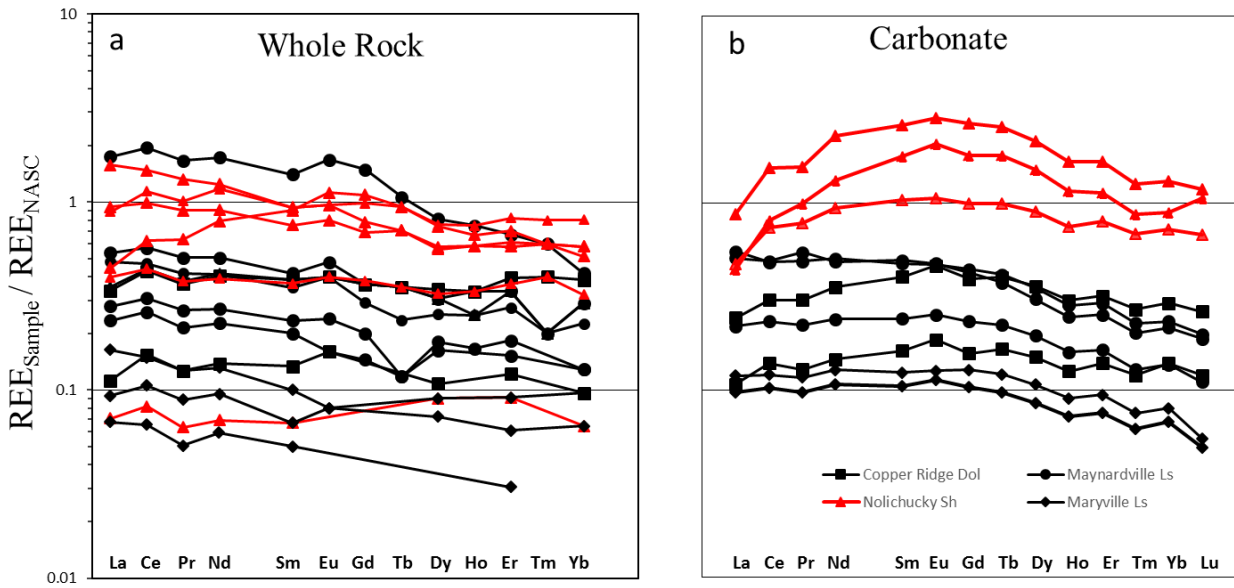


Figure 8: NASC-normalized rare earth element concentrations in a) whole rock samples and b) carbonate leached with acetic acid.

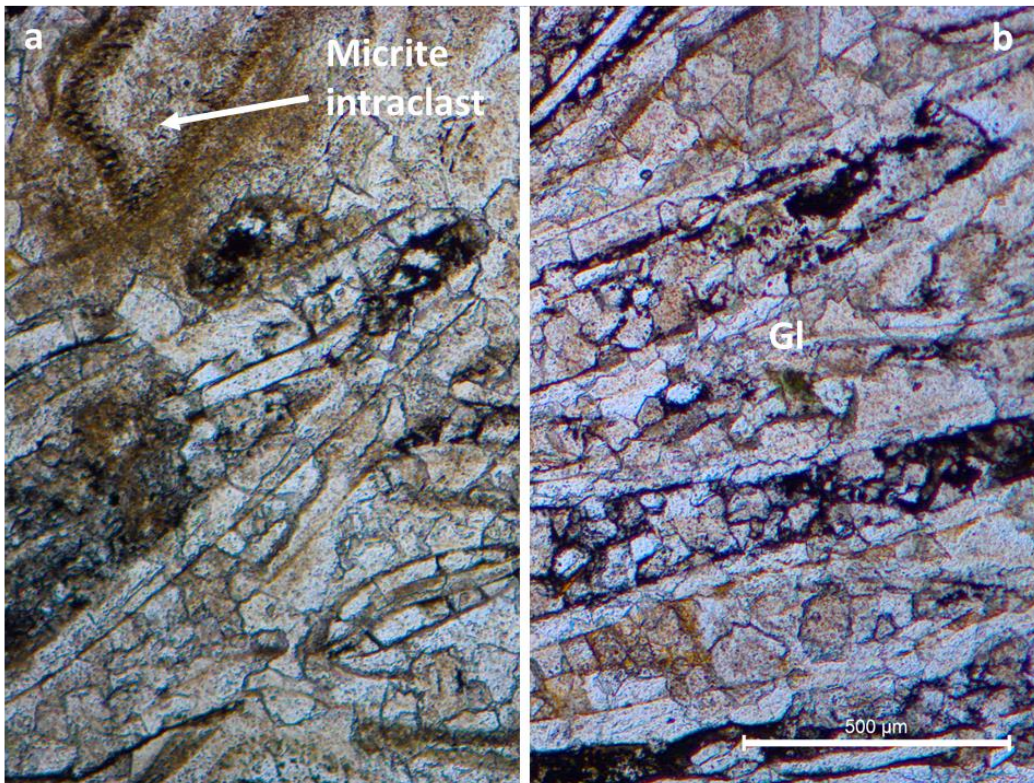


Figure 9: Plane polarized photomicrographs of sample 0714ARIS5060. a) sparry dolomite and oxide rimmed micrite intraclast; b) sparry filled laminoid fenestrate texture.

resulted in higher Σ REE and partial oxidation of any sulfide that was present (Aller and Rude, 1988; Öztürk, 1995; Dong et al., 2000; Schippers and Jørgensen, 2001).

The REE patterns of carbonate leached from the Nolichucky and Copper Ridge Formations (Figure 8b) exhibit a positive cerium anomaly ($[Ce/Ce^*]_{SN}$), calculated after the method of Bau and Dulski (1996) where

$$(Ce/Ce^*)_{SN} = Ce_{SN} / (0.5La_{SN} + 0.5Pr_{SN})$$

and SN indicates shale-normalized values. Positive $(Ce/Ce^*)_{SN}$ ratios can result from anomalous La enrichment. A solution to this is to plot the $(Ce/Ce^*)_{SN}$ versus $(Pr/Pr^*)_{SN}$, where:

$$(Pr/Pr^*)_{SN} = Pr_{SN} / (0.5Ce_{SN} + 0.5Nd_{SN})$$

A true positive Ce anomaly plots as $(Ce/Ce^*)_{SN} > 1$ and $(Pr/Pr^*)_{SN} < 1$. The positive $(Ce/Ce^*)_{SN}$ occurring within the Nolichucky Formation and Copper Ridge Formation are shown in Figure 10.

Figure 11 shows the variance of U and Mn between the whole rock and carbonate fractions. Whole rock U concentrations fluctuate within the sample interval, first peaking within the clastic rich facies of the upper Nolichucky Formation and then again within the Maynardville Formation at ~1560 meters. The U concentrations within the carbonate fraction show a different trend than those of the whole rock. Carbonate-hosted U peaks at 1.39 mg kg⁻¹ at 1561 m and then continually drops to 0.03 mg kg⁻¹ at the top of our study interval. Whole rock Mn concentrations have a range of 532 to 740 mg kg⁻¹ within the Nolichucky Formation with a large

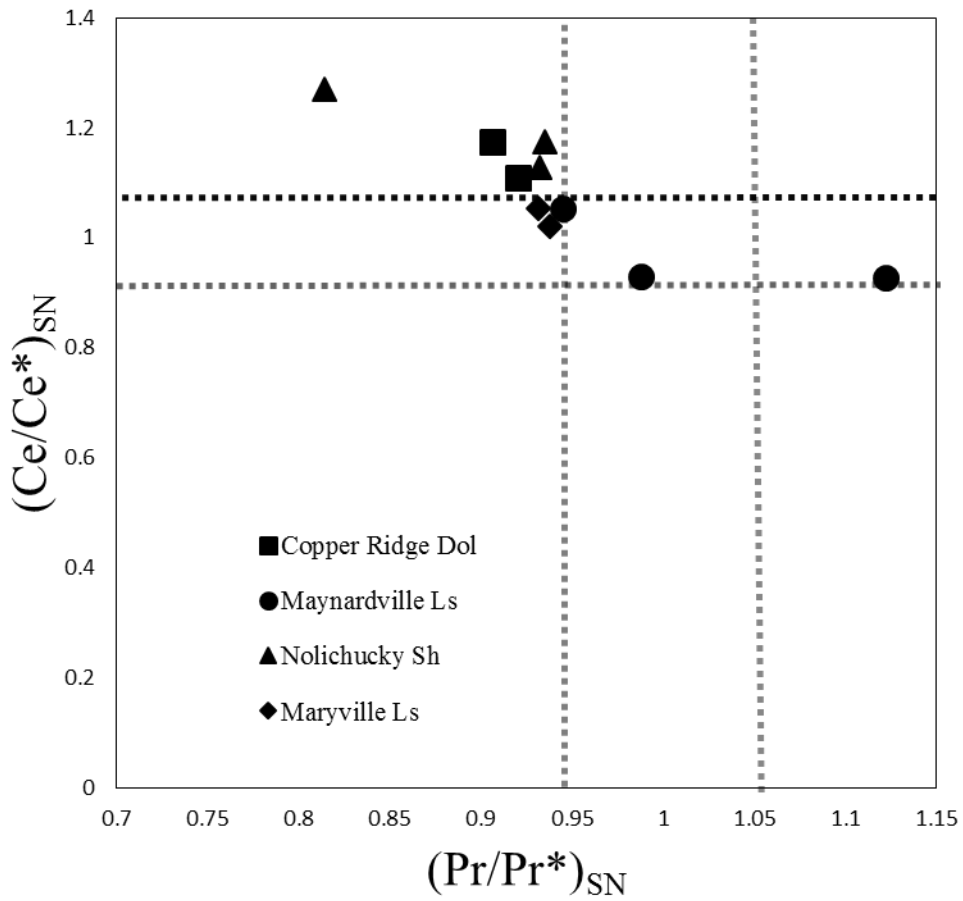


Figure 10: NASC normalized true Ce/Ce* anomaly plotted versus Pr/Pr* after Bau and Dulski, (1996). Samples plotted in the upper left hand segment are true Ce/Ce* anomalies.

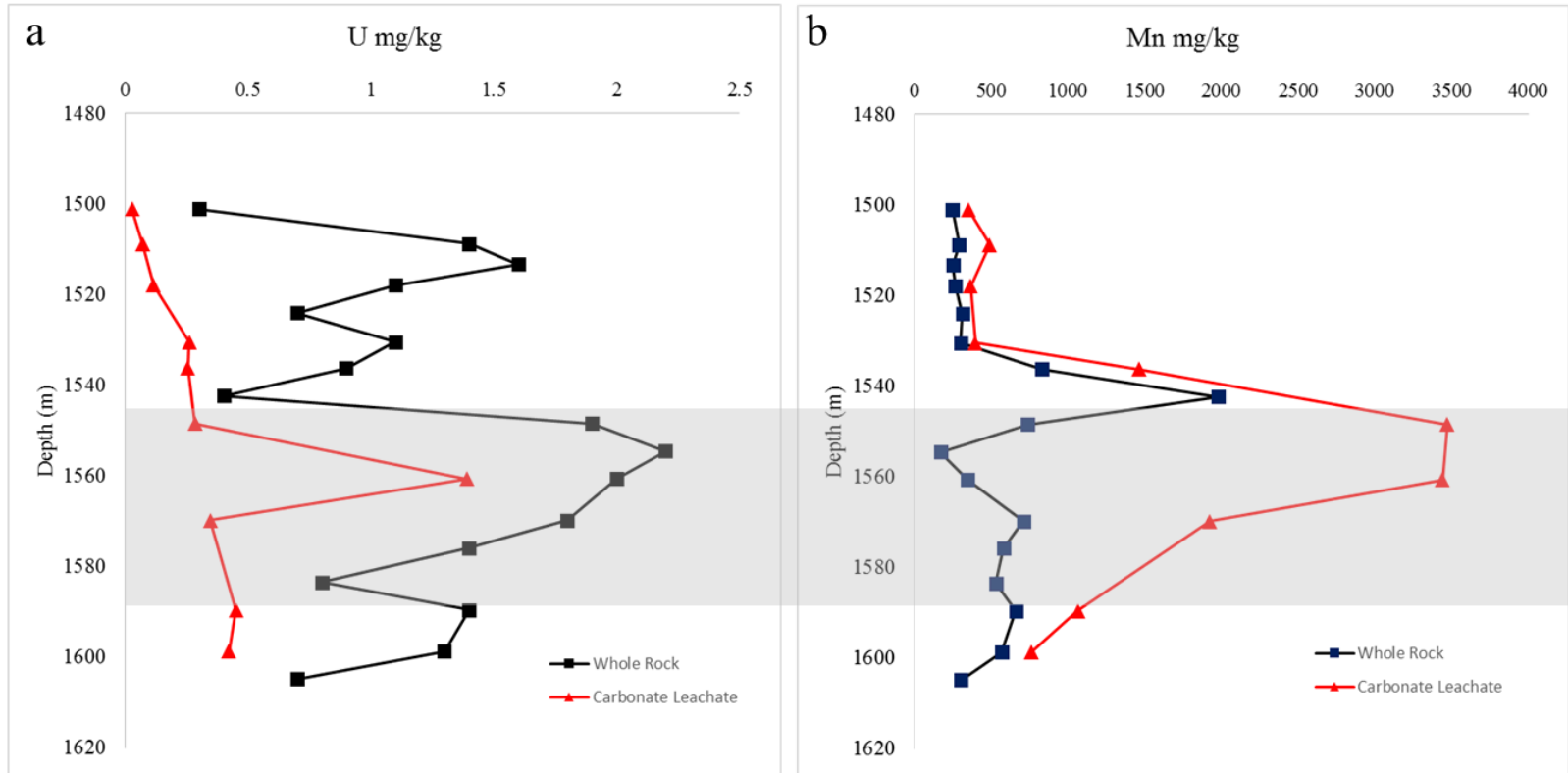


Figure 11: Variations in U and Mn in whole rock and carbonate samples as a function of depth. a) Uranium concentrations in both whole rock and carbonate are low; U in the carbonate shows a systematic decrease upward (with the exception of the Nolichucky Formation sample at 1560 m), while the whole rock is more variable. b) Manganese concentrations are significantly elevated in the carbonate over the interval of 166-1550 m. The Nolichucky Formation is highlighted in grey.

increase at 1542 m (sample 0715ARIS5060) and then decrease to a range of 314 to 250 mg kg⁻¹ for during the upper Maynardville and Copper Ridge Formations. The Mn concentrations within the carbonate fraction are significantly elevated (1066 to 3471 mg kg⁻¹) within the Nolichucky Formation and lower subtidal facies within the Maynardville Formations relative to the whole rock compositions.

4.4 STABLE ISOTOPES

The $\delta^{13}\text{C}$ and $\delta^{18}\text{O}$ values are reported in Table 7. A slight positive $\delta^{13}\text{C}$ trend starts in the Maryville Formation and into the basal dolomite portion of the Nolichucky Formation with values ranging from -1.25 to -0.97‰. A more rapid $\delta^{13}\text{C}$ excursion starts at ~1585 meters depth (-0.97‰) up to 1563 m (0.56‰). The next sample at 1551 m is -0.3‰, showing a slight negative excursion and then continuing with a positive $\delta^{13}\text{C}$ excursion to a maximum value of 4.03‰ at the contact between the Maynardville Formation and the Copper Ridge Formation. The excursion then decreases slightly to 2.94‰ at the top of the study interval.

$\delta^{18}\text{O}$ values were calculated relative to the V-PDB standard, and fell within a range of 6.74‰ in the fossiliferous section of the Maynardville Formation to 5.07‰ in the Nolichucky Formation. These values are significantly lower than the range of values (9.34 to 5.99‰) measured in the Conasauga Group from outcrops in the Tennessee Valley and Ridge Province. This variation is likely the result of diagenetic alteration when the primary calcite was replaced by dolomite.

Table 7: $\delta^{13}\text{C}$, $\delta^{18}\text{O}$, measured and age corrected $^{87/86}\text{Sr}$ of carbonate. $\delta^{13}\text{C}$ and $\delta^{18}\text{O}$ values were measured via IRMS and reported permil relative to V-PDB. $^{87/86}\text{Sr}$ values were measured on MC-ICP-MS. Age corrected $^{87/86}\text{Sr}$ values were calculated using 497 ma.

Depth m	Sample Number	$\delta^{13}\text{C}$	$\delta^{18}\text{O}$	Measured $^{87/86}\text{Sr}$	Age Corrected $^{87/86}\text{Sr}$
1494	0715ARIS 4900	2.94	-5.59		
1501	0715ARIS 4925	3.77	-5.47	0.709305	0.709275
1509	0715ARIS 4950	3.55	-5.63	0.709632	0.709571
1510	0715ARIS 4955	3.43	-5.89		
1513	0715ARIS 4965	3.72	-5.70		
1515	0715ARIS 4970	4.00	-5.70		
1518	0715ARIS 4980	3.84	-5.87	0.709615	0.709463
1521	0715ARIS 4990	4.03	-5.69		
1524	0715ARIS 5000	3.52	-5.84		
1527	0715ARIS 5010	3.20	-6.26		
1530	0715ARIS 5021	2.63	-6.74	0.709469	0.709364
1533	0715ARIS 5030	2.89	-5.42		
1536	0715ARIS 5040	2.52	-5.91	0.710056	0.709862
1539	0715ARIS 5050	1.24	-5.69		
1542	0715ARIS 5060	0.98	-6.03		
1545	0715ARIS 5070				
1548	0715ARIS 5080	0.39	-6.23	0.712822	0.712334
1551	0715ARIS 5090	-0.30	-6.62		
1554	0715ARIS 5100				
1558	0715ARIS 5110				
1561	0715ARIS 5120			0.714981	0.713530
1564	0715ARIS5130	0.56	-5.87		
1570	ARIS 5150	0.25	-5.07	0.714260	0.713344
1576	ARIS 5170	-0.28	-6.35		
1583	ARIS 5195	-0.91	-6.26		
1590	ARIS 5215	-0.97	-6.12	0.709792	0.709607
1599	ARIS 5245	-1.17	-5.81	0.710067	0.709698
1605	ARIS 5265	-1.25	-5.94		

* δ values calculated relative to VPDB

4.5 STRONTIUM ISOTOPE STRATIGRAPHY

Measured carbonate (acetic acid leachate) $^{87}\text{Sr}/^{86}\text{Sr}$ values (Table 7) were corrected for decay of rubidium since the Late Cambrian (494 Ma.) based on the carbonate Rb and Sr data (Table 4). The $^{87}\text{Sr}/^{86}\text{Sr}$ values in the carbonate units fall near, but slightly above, expected values for Cambrian seawater (e.g., Montanez et al., 1996). The values from carbonate cement extracted from the Nolichucky Formation samples ARIS5150, 0715ARIS5120 and 0715ARIS5080 are considerably more radiogenic than the underlying and overlying carbonate.

5.0 DISCUSSION

5.1 DIAGENESIS AND GEOCHEMICAL PRESERVATION

5.1.1 Late Cambrian seawater carbon and strontium signals

Much of the carbonate in the samples used in this study has undergone some degree of secondary replacement by dolomite during the initial shallow burial of the sediments. The presence of authigenic microcline within the samples also suggests potassium-rich brine migration and perhaps metasomatism during the Alleghanian Orogeny (Hearn and Sutter, 1985a). Transport and diffusion characteristics on the system (e.g., porosity, permeability, and reactive surface area) can significantly affect trace element and isotopic signatures (Jonas et al., 2017). The degree to which marine carbonate preserves its original seawater Sr isotope composition can be used to assess the degree of alteration in carbonate samples used in carbon isotope studies (Derry et al., 1992). Samples taken from the Maryville, Maynardville and Copper Ridge Formations are slightly more radiogenic (Figure 12) than previously recorded values ($^{87}\text{Sr}/^{86}\text{Sr} = 0.70917\text{-}0.70930$) of coeval Upper Cambrian marine carbonate strata (Montañez et al., 1996; Denison et al., 1998). The age-corrected value for our Copper Ridge Formation samples (0.70957-0.70927) are close to those reported in coeval rocks from the Great Basin (Saltzman et al., 1995). This implies that the carbonate trace element signatures can be interpreted primarily as Late Cambrian

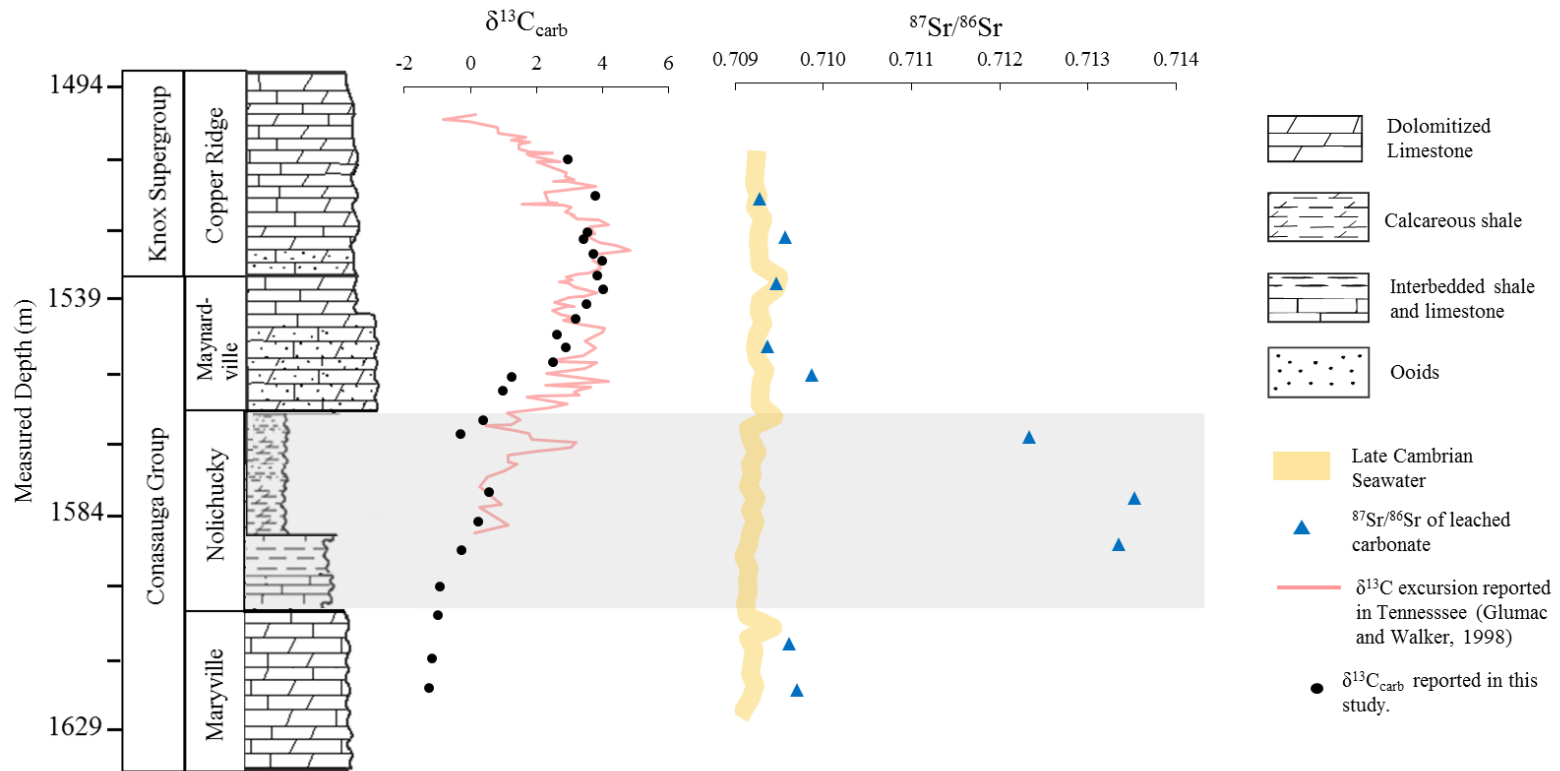


Figure 12: $\delta^{13}\text{C}$ values of the study samples (black circles) plotted with depth-adjusted values of Glumac and Walker (1998) in red. Blue circles are age corrected $^{87}\text{Sr}/^{86}\text{Sr}$ isotope ratios measured in leached carbonate of our sample set. Shaded line (grey) is depth-adjusted average Late Cambrian seawater (Montanez et al., 1996)

seawater proxies without significant influence from diagenetic overprinting or later fluid flow events. The $^{87}\text{Sr}/^{86}\text{Sr}$ values measured in carbonate extracted from the Nolichucky Formation are much too radiogenic to reflect Late Cambrian seawater; these likely recorded the signal of carbonate precipitated out of shale pore waters that had previously reacted with Rb-rich aluminosilicates.

The $\delta^{13}\text{C}_{\text{carb}}$ excursion reported in this study was determined on both bulk carbonate and carbonate cement from a variety of depositional environments. As interpreted from the $^{87}\text{Sr}/^{86}\text{Sr}$ values, dolomicrite within the shale-dominated sections of the Nolichucky Formation were likely precipitated from pore-water bicarbonate. There is potential to decrease $\delta^{13}\text{C}_{\text{carb}}$ values through organic-matter degradation via microbially mediated reduction, methanogenesis, and thermal decarboxylation during burial diagenesis (Claypool and Kaplan, 1974; Irwin et al., 1977; Saltzman and Thomas, 2012). The influence of such processes could result in a decrease in the $\delta^{13}\text{C}_{\text{carb}}$ excursion, and the short, negative excursion within the upper Nolichucky Formation (1554 m) could be the result of such processes. However the persistent positive $^{13}\text{C}_{\text{carb}}$ values similar those found within the overlying carbonate and other formations where SPICE has been documented likely indicate the dolomicrite within the shale facies precipitated relatively early in its diagenetic history and maintains the Late Cambrian seawater $\delta^{13}\text{C}$.

5.1.2 Trace element signatures in carbonate

Carbonate dissolution in dilute acetic acid has in some cases resulted in leaching of trace elements from detrital material and Fe-Mn oxides (Zhang et al., 2015; Tostevin et al., 2016). Partial leaching of Fe-Mn oxides and silicate (mostly clays) can mask primitive seawater signals (Bau, 1999;

Shields and Webb, 2004; Ling et al., 2013). Any correlation of Mn, Fe or Al with the REE can be recognized using simple regression analysis between the elemental constituents in the bulk rock and resulting contaminant (Fig. 13). There is no appreciable correlation between Mn and Al concentrations in the bulk rock data (Fig. 13a), which suggests that the Mn concentrations are not hosted in aluminosilicates. The moderate correlation between Fe and Al (Fig. 13b) within the Nolichucky Formation in the whole rock data is likely due to the presence of glauconite (Fig. 5h). There is no apparent correlation between Mn and Fe concentrations in the bulk rock (Fig. 13c) implying Fe-Mn oxides are sparse or absent. The lack of correlation between bulk rock Mn concentration and iron or total REE of the carbonate (Fig. 13d) show no apparent correlation. Mn oxyhydroxides are known to scavenge REE from seawater and any partial dissolution would dramatically influence the total REE abundance and subsequent pattern. There a correlation between carbonate hosted Mn and $\Sigma\text{REE}_{\text{carb}}$ (Fig. 13e), primarily in carbonate within the Nolichucky Formation, which has been shown to be diagenetic rather than primary. Mn oxyhydroxides are known to preferentially scavenge Ce from the water column in oxidizing conditions (Alibo and Nozaki, 1999; Ling et al., 2013; Tostevin et al., 2016). The absence of correlation between Ce/Ce* and whole rock Mn or Al concentrations (Fig. 13f-g) argues against release of REE by partial leaching of Mn-oxides. There could be an influence on the carbonate REE signature in sections with high amounts of clay, particularly in the Nolichucky Formation (Fig. 13h).

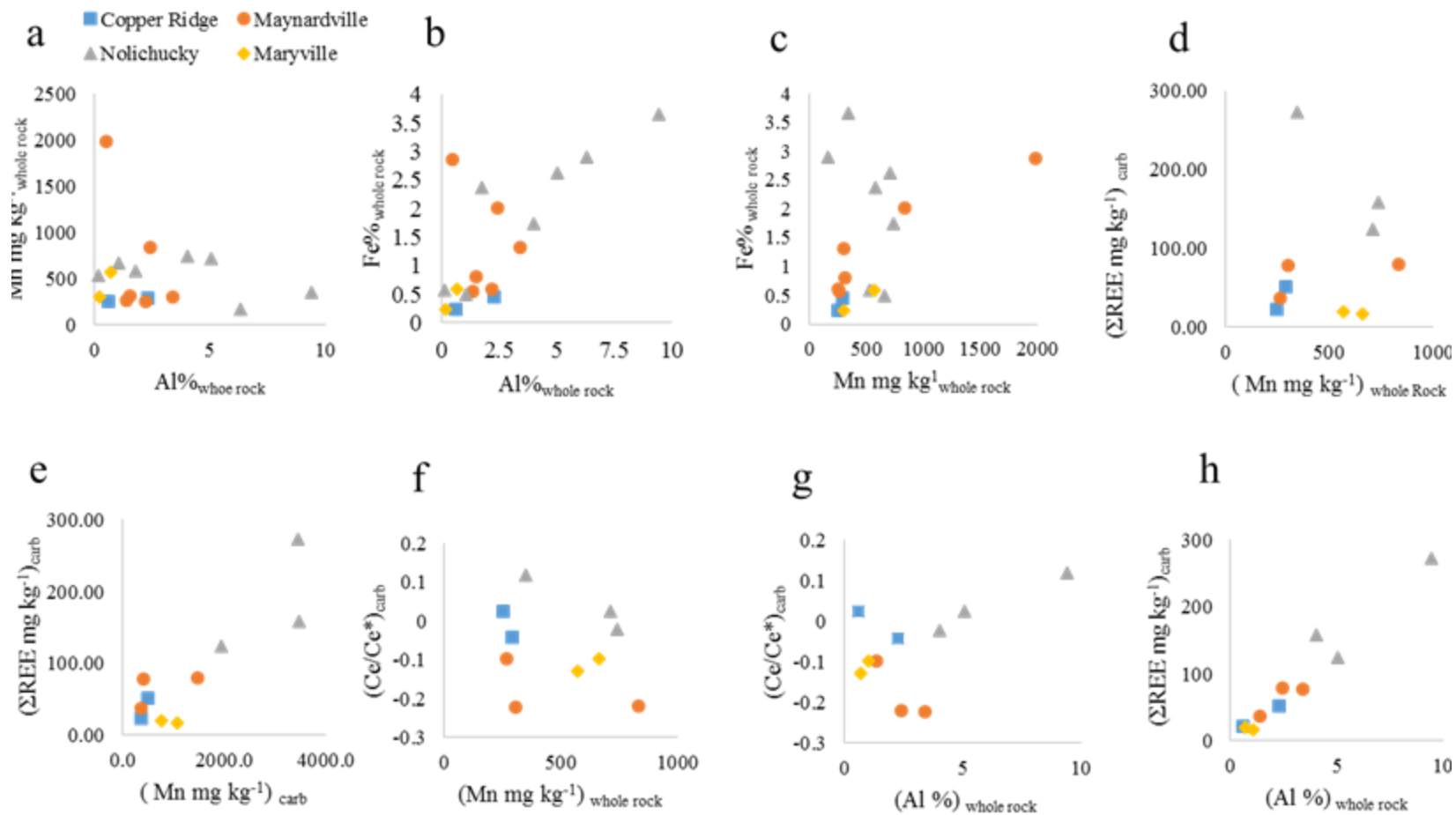


Figure 13a-h: Regression analysis of common geochemical contaminant signatures. (a-b): Whole rock Mn mg kg⁻¹ and Fe % plotted versus whole rock Al%; (c): Whole rock Fe% versus whole rock Mn mg kg⁻¹; (d): whole rock Mn mg kg⁻¹ vs ΣREE of carbonate; (e): Mn mg kg⁻¹ vs. ΣREE mg kg⁻¹ of the carbonate. Carbonate Ce/Ce* plotted versus (f) whole rock Mn mg kg⁻¹ and (g) whole rock Al% (h): Carbonate ΣREE plotted versus whole rock Al%.

5.2 CARBON ISOTOPE CHEMOSTRATIGRAPHY AND CORRELATION

The sample interval shows a $\delta^{13}\text{C}_{\text{carb}}$ excursion comparable in magnitude to other correlative $\delta^{13}\text{C}$ excursions around the globe (Saltzman et al., 1998; Saltzman et al., 2000b; Kouchinsky et al., 2008; Ahlberg et al., 2009; Woods et al., 2011). The robustness of the $\delta^{13}\text{C}_{\text{carb}}$ excursion measured in this study seems to be relatively unaffected by mineralogical and diagenetic alteration, having a continuous positive progression through both biogenic and matrix cement carbonate. There is a small facies influence on the positive $\delta^{13}\text{C}_{\text{carb}}$ excursion in our samples within upper clastic-dominated Nolichucky Formation. However, positive $\delta^{13}\text{C}_{\text{carb}}$ values persist through siliciclastic-dominant subtidal, intertidal and finally supratidal facies. In addition, it conforms well to $\delta^{13}\text{C}_{\text{carb}}$ values measured in the Conasauga Group ~200 miles south, on the other side of the Rome Trough (Fig. 12) (Hasson and Haase, 1988b; Glumac and Walker, 1998; Glumac and Mutti, 2007).

Comparison of our curve and $\delta^{13}\text{C}_{\text{carb}}$ values taken in coeval strata sampled in the southern Appalachian basin (Glumac and Walker, 1998) shows similar maximum values (~4-5‰) at the contact between the Maynardville and Copper Ridge Formations. The C isotope excursion is observed at both sites over a burial depth of ~100 m (Fig 12). However, $\delta^{13}\text{C}_{\text{carb}}$ in the carbonate fraction within the Nolichucky Formation shale at our site is lower (-0.27 to +0.98‰) than to those reported south of the Rome Trough for similar dolomicrite (0.116 to 1.37; Glumac and Walker 1998). Although Late Cambrian terrestrial systems lacked contributions from vascular plants, sediment loads and salinity differences could have played a role in localized $\delta^{13}\text{C}$ fractionation

It is likely that the variation observed in our samples reflects closer proximity to Laurentian deltaic sediments than those studied at the southern site (Fig. 2) (Janssens, 1973). It is notable that despite mixed sediment sources and basin proximity, the Late Cambrian C isotope excursions at both Appalachian sites are comparable in magnitude to other SPICE related $\delta^{13}\text{C}_{\text{carb}}$ excursions around the globe (Saltzman et al., 2000a; Kouchinsky et al., 2008; Ahlberg et al., 2009; Gill et al., 2011; Woods et al., 2011; Ng et al., 2014).

It is believed that positive $\delta^{13}\text{C}$ excursions are caused by the removal isotopically light ^{12}C during increased organic matter deposition and preservation, or by the weathering of heavy $\delta^{13}\text{C}$ hosted rocks (such as carbonate) (Saltzman and Thomas, 2012). The positive $\delta^{13}\text{C}_{\text{carb}}$ excursion in this study coincides with a global increase in sea level, referred to as the Sauk Transgression in Laurentia (Glumac and Walker, 2000; Saltzman et al., 2004). Transgressions of this magnitude resulted in epeiric seas, reducing the amount of surface area exposed to weathering, thus mitigating any weathering-related heavy carbon fluxes in the ocean. Also, mantle- and lithosphere-derived carbon emitted via volcanoes would have been isotopically light (-5‰) and have a net negative influence on the isotope trend (Saltzman and Thomas, 2012).

There has also been speculation about anomalous $\delta^{13}\text{C}$ excursions resulting from mineralogical changes during diagenesis (Railsback et al., 2003; Saltzman and Thomas, 2012; Fantle and Higgins, 2014). The SPICE is a global phenomenon of nearly equal magnitude, recorded in multiple sedimentary environments. Synchronous diagenetic alteration on a global scale is considered to be highly unlikely. Therefore, we interpret the positive $\delta^{13}\text{C}_{\text{carb}}$ trend as the result of the removal of isotopically light ^{12}C with increased organic carbon burial and preservation (Kump and Arthur, 1999; Saltzman and Thomas, 2012).

5.3 TRACE ELEMENT CYLCE DISRUPTIONS DUE TO SPICE

5.3.1 Evidence of anoxia on Laurentian passive margin?

Discerning the paleoredox conditions of ancient marine carbonate and siliciclastic sediments requires a multiproxy approach (Jones and Manning, 1994; Tribovillard et al., 2006; Schröder and Grotzinger, 2007; Azmy et al., 2015). Iron concentrations are widely used in the study of redox systems and have been proven a reliable indicator of anoxic and euxinic conditions in both modern and ancient systems (Lyons and Severmann, 2006). One mechanism for Fe transfer driven by redox changes involves Fe(II) being decoupled and mobilized from detrital material on the shallow shelf and redeposited in a deeper euxinic basin as syngenetic pyrite (Canfield and Teske, 1996; Raiswell and Canfield, 1998; Lyons and Severmann, 2006). The ratio of total Fe ($Fe_T = Fe^{2+} + Fe^{3+}$) to Al is a useful proxy for determining the enrichment in reactive Fe relative to Fe in the clastic portion of the sediments. Broadly, Fe_T/Al mass ratios >0.5 (average crustal value; Taylor and McLennan, 1985) suggest anoxic depositional conditions. The Fe_T/Al ratios in the samples reported here display alternating oxic and anoxic signals within the subtidal Nolichucky Formation and up through the lower, peritidal facies within the Maynardville Formation (Fig. 14). The highest Fe_T/Al ratio (5.9) was recorded at ~1542 m (sample 0715ARIS5060) within the lower Maynardville Formation. Figure 9 is a photomicrograph taken of the sample showing abundant bioclasts and oxide rimmed micrite intraclasts that likely

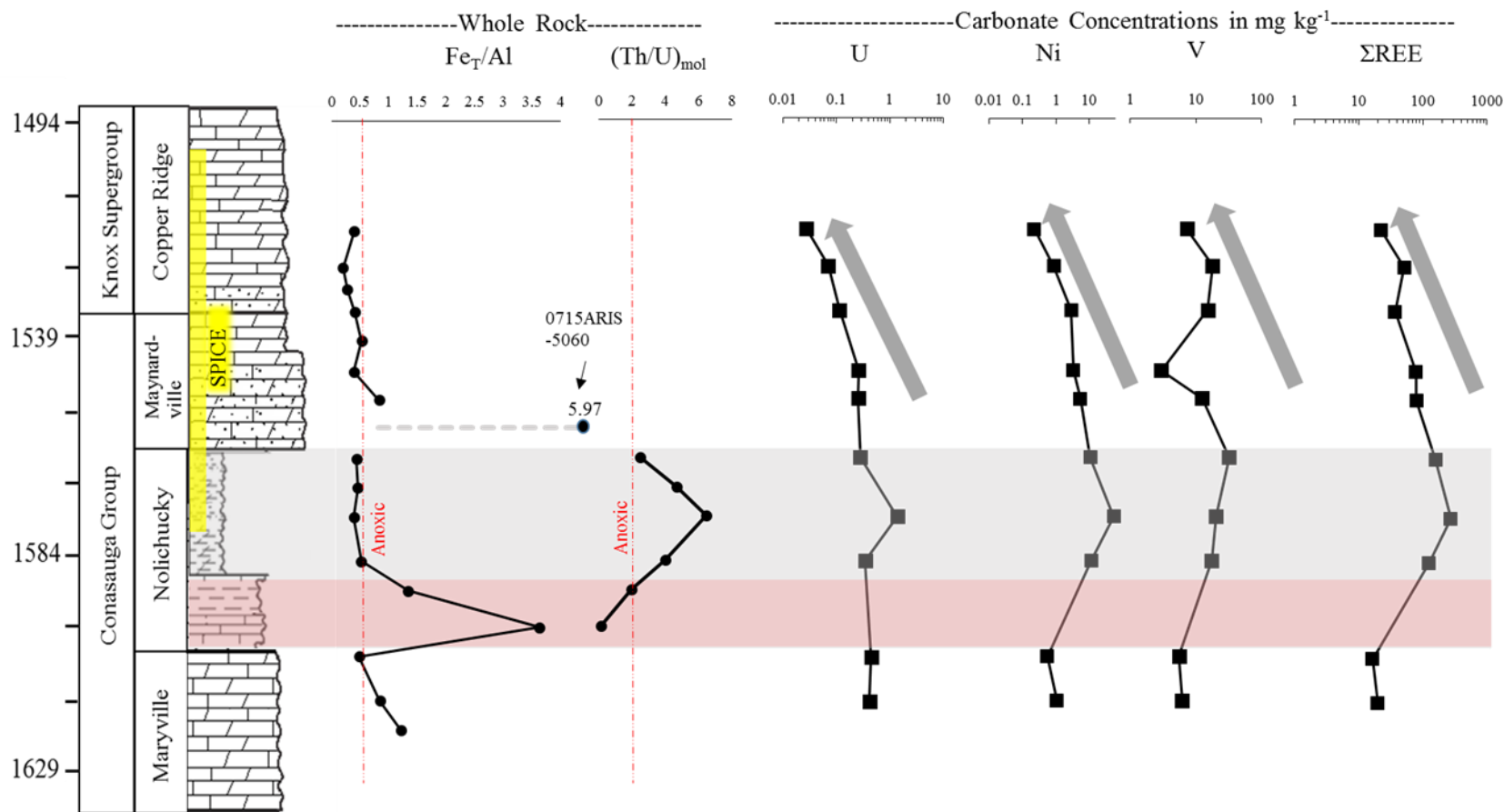


Figure 14: Fe_T/Al and Th/U mol of whole rock samples. Carbonate U, Ni, V and ΣREE are concentrations plotted on logarithmic scale with depth and stratigraphy. The SPICE interval within our sample set is highlighted in yellow. The Nolichucky Formation is highlighted in grey. Overlap of Fe_T/Al and Th/U values that indicate anoxic conditions is highlighted in red.

concentrated iron and manganese in the sample as discussed in section 4.3. The Maynardville Formation marks the transition to an oxic supratidal environment and the anomalously high Fe_T/Al ratios in the lower half of the section likely result from biological and physical reworking, which can concentrate labile iron within the sediments (Lyons and Severmann, 2006). The second and third highest values (3.65 and 1.33) were found in succession in the lower Nolichucky Formation. The Fe_T/Al ratios within the deeper Nolichucky Formation shows strong evidence of an anoxic water column contemporaneous to the start of SPICE at our sample location.

The ratio of Th/U can be a useful paleoredox proxy in siliciclastic sediments, given that U^{6+} in the soluble uranyl carbonate ion ($U^{VI}O_2^{2+}$) is reduced to insoluble U^{4+} in suboxic and anoxic conditions (Wignall and Twitchett, 1996). Ratios of Th/U <2 imply accumulation of U in the sediments under anoxic conditions (Wignall and Twitchett, 1996). Th/U molar ratios in the Nolichucky Shale are plotted with depth in Figure 14. Ratios fall within the anoxic range contemporaneous to the sedimentation shift from the Maryville Formation to the lower facies of the Nolichucky Formation (1583 – 1576 m). This interval precedes the start of the $\delta^{13}C_{carb}$ excursion (SPICE) in our sample set. A subsequent increase in Th/U suggests more oxic conditions from 1576 m to the contact between the Nolichucky and Maynardville Formations. Deposition of this sequence in an oxygenated environment could have resulted from shallowing of the study area during the Sauk II-III Sub-regression.

5.3.2 Regional and global oceanic trace element fluctuations during SPICE

Persistent anoxia similar to that associated with SPICE could lead to a global drawdown in seawater trace element inventories (Anbar and Knoll, 2002; Saito et al., 2003; Algeo, 2004). Many redox-sensitive trace elements exhibit a higher rate of transfer from seawater and accumulation in

the underlying sediments in reducing conditions, and because of this phenomenon, oceanic trace element residence times and concentrations were shorter during large-scale ocean anoxia in the Paleozoic than in modern oxygenated seawater (Algeo, 2004). The Alum Formation of Sweden consists of organic rich shales spanning the Middle to Late Cambrian and contains a positive $\delta^{13}\text{C}_{\text{org}}$ excursion and a decline in Mo concentrations concomitant with the progression of SPICE (Gill et al., 2011). Molybdenum concentrations within our study samples were below analytical detection limit and well below those measured within the coeval Alum Formation of Sweden (Gill et al., 2011). However, our samples show an upward decline in U and Ni concentrations, with an exception at 1560 m, within the leached carbonate fraction beginning with the deposition of the Nolichucky Formation (Figs. 11, 14).

A similar trend can be interpreted by the behavior of Mn in the study samples. Mn^{2+} and $\text{Mn}^{\text{Cl}+}$ are the main species in seawater, and these species are thermodynamically unstable in oxygenated surface waters and precipitate out as Mn-oxyhydroxides. Beneath the oxic-anoxic chemocline, Mn-oxyhydroxides undergo reductive dissociation, mobilizing soluble Mn^{2+} (Tribovillard et al., 2006). The Mn^{2+} is not readily immobilized in sulfide phases, so upward or downward diffusion can occur (Tribovillard et al., 2006). Whole rock Mn concentrations are relatively stable except for a decrease in concentration between ~1565 to 1554 m depth (Fig. 11). During that interval, Mn concentrations in carbonate fraction increase significantly. This suggests that Mn may have undergone reductive mobilization as soluble Mn^{2+} . Any Mn^{2+} that didn't escape the sediment column could have been trapped in the authigenic carbonate minerals forming at the time. If these sediments were deposited under oxic conditions, we would expect to see accumulation of Mn in the whole rock sediments and a drawdown in the carbonate fraction as insoluble Fe-Mn oxyhydroxides precipitated out of the water column and sedimentary porewaters.

The behavior of Mn whole rock and carbonate fractions suggest a local reducing environment during or shortly after deposition.

An important implication of trace element drawdowns from black shale deposition is the bioavailability of limiting nutrients and its effects on biologic evolution. The transition metals V, Ni, Mo and Fe are vital to the biochemical processes related to nitrogen fixation and organic productivity, and have been linked to eukaryote development during the late Proterozoic (Anbar and Knoll, 2002). Dissolved Ni is incorporated into organic matter through organo-metallic bonds and transferred to the sediment column through deposition of organic matter and sulfide mineralization. Nickel can be remobilized in during organic matter decay and recycled back into the water column (Tribovillard et al., 2006). However, Ni and other trace metals can accumulate in sediments during enhanced organic matter deposition and preservation in anoxic black shale facies, such as that postulated during the SPICE. Longer periods of ocean anoxia can lead to a drawdown of dissolved Ni and other trace metals due to their immobilization in sedimentary sulfide minerals (Algeo, 2004; Tribovillard et al., 2006). Our samples show an upward decline in Ni and Fe concentrations (Figs. 7,14) within the leached carbonate fraction coeval with the progression of the positive $\delta^{13}\text{C}_{\text{carb}}$ excursion. Remobilization of trace elements during diagenesis or Alleghenian metasomatism is possible and values within Nolichucky Formation carbonate may be affected by interaction with the clastic component. Nonetheless, the continued reduction within the overlying carbonate units could indicate a drawdown in dissolved trace metals in the Late Cambrian oceans as Ni is removed through production of organic matter and then immobilized in a euxinic basin proximal to our study location (Algeo, 2004). Perturbations to trace element bioavailability may have had an effect on nutrient fluxes within the marine system, and possibly

influenced productivity in the post-SPICE oceans (Anbar and Knoll, 2002; Anbar, 2008; Brennecke et al., 2011).

5.3.3 Late Cambrian seawater rare earth element chemistry

Whole rock REE concentrations normalized to the North American Shale Composite (NASC) display patterns broadly consistent with an upper crustal source (Fig. 8a). REE patterns in the carbonate units (Maryville and Maynardville Limestone and Copper Ridge Dolomite; Fig. 8b), are similar to those of their associated whole rocks, and do not resemble NASC-normalized modern seawater (Webb and Kamber, 2000), which is depleted in light rare earth elements and displays a negative Ce anomaly (Bau and Dulski, 1996). There is debate regarding the extent to which seawater REE composition has changed through time (Webb and Kamber, 2000; Nothdurft et al., 2004; Shields and Webb, 2004; Meyer et al., 2012). Reduced LREE and Ce depletion could be associated with dolomitization during early diagenesis if there were reducing porewaters (Nothdurft et al., 2004).

The REE pattern of carbonate leached from the Nolichucky and Copper Ridge Formations (Fig. 8b) exhibit a positive $(\text{Ce}/\text{Ce}^*)_{\text{SN}}$ anomaly (Fig. 10). Cerium is preferentially scavenged from seawater during the formation of Fe-Mn oxides in an oxygenated water column. This leaves oxygenated seawater with a negative Ce/Ce* anomaly. Cerium is released in anoxic sediments by reductive dissolution of the oxides across the oxic/anoxic boundary, or in the presence of reducing pore waters during early diagenesis (Alibo and Nozaki, 1999; Bau, 1999; Abanda and Hannigan, 2006; Ling et al., 2013).

6.0 CONCLUSION

Core samples from the Conasauga Group and overlying Knox Supergroup of the Central Appalachian basin preserve Late Cambrian seawater geochemical proxies in both carbonate and clastic sediments. The paleogeographic location of the samples suggests deposition on the shallow, craton-ward side of a deep extensional basin off Laurentia, making the sedimentary environment highly influenced by Iapetus Ocean sea-level fluctuations during the Sauk II-III Super-sequence. Strontium isotopes in carbonate sequences yield values near those expected for Late Cambrian seawater, despite dolomitization and possible metasomatic fluxes of K-bearing fluids. Carbonate cement in the shale units of the Nolichucky Formation show evidence of interaction with a high-Rb clastic component.

A trend of upward increasing $\delta^{13}\text{C}_{\text{carb}}$ can be attributed to the Steptoean Positive Carbon Isotope Excursion (SPICE), and it is comparable in magnitude to $\delta^{13}\text{C}$ excursions recorded in other parts of Laurentia (Glumac and Walker, 1998; Saltzman et al., 1998). The correlation of $\text{Fe}_\text{T}/\text{Al}$, Th/U and positive Ce/Ce^* within shales of the Nolichucky Formation immediately preceding SPICE strongly suggests an initial anoxic water column (Wignall and Twitchett, 1996; Lyons and Severmann, 2006; Tribovillard et al., 2006; Schröder and Grotzinger, 2007; Tostevin et al., 2016) just prior to the onset of the SPICE. This was followed by a sea level fall resulting in a more oxic depositional environment. A temporal decrease in carbonate hosted U concentrations up through the Nolichucky Formation and into the overlying Maynardville and Copper Ridge Formations contemporaneous with the SPICE could indicate a global drawdown in soluble trace metals in response to extensive black shale deposition. Our sample has low TOC content (<0.5%), however decreasing trends in Ni and ΣREE measured in the leached carbonate portion could signal a

regional drawdown of soluble concentrations as a result of black shale deposition deeper in the Rome Trough and adjacent Conasauga intrashelf basin.

7.0 SUMMARY

- 1) The data suggest anoxic conditions were present on the shallow continental shelf of Laurentia pencontemporaneous to the start of a positive $\delta^{13}\text{C}_{\text{carb}}$ excursion at the study site.
- 2) Upward decreasing trends in Ni and ΣREE concentrations within the carbonate can be interpreted as occurring as the result of a seawater-drawdown in response to regional organic rich shale deposition, despite the low (<0.5%) TOC content within our sample set.
- 3) A temporal decrease in U measured in leached carbonate is interpreted as a drawdown in Late Cambrian Ocean concentrations in response to global deposition of black shale contemporaneous to SPICE.

BIBLIOGRAPHY

- Abanda, P. A., & Hannigan, R. E. (2006). Effect of diagenesis on trace element partitioning in shales. *Chemical Geology*, 230(1-2), 42-59. doi:10.1016/j.chemgeo.2005.11.011
- Ahlberg, P., Axheimer, N., Babcock, L. E., Eriksson, M. E., Schmitz, B., & Terfelt, F. (2009). Cambrian high-resolution biostratigraphy and carbon isotope chemostratigraphy in Scania, Sweden: first record of the SPICE and DICE excursions in Scandinavia. *Lethaia*, 42(1), 2-16.
- Algeo, T. J. (2004). Can marine anoxic events draw down the trace element inventory of seawater? *Geology*, 32(12), 1057. doi:10.1130/g20896.1
- Alibo, D. S., & Nozaki, Y. (1999). Rare earth elements in seawater: particle association, shale-normalization, and Ce oxidation. *Geochimica et Cosmochimica Acta*, 63(3), 363-372.
- Aller, R. C., & Rude, P. D. (1988). Complete oxidation of solid phase sulfides by manganese and bacteria in anoxic marine sediments. *Geochimica et Cosmochimica Acta*, 52(3), 751-765.
- Anbar, A. D. (2008). Elements and evolution. *Science*, 322(5907), 1481-1483.
- Anbar, A. D., & Knoll, A. (2002). Proterozoic ocean chemistry and evolution: a bioinorganic bridge? *Science*, 297(5584), 1137-1142.
- Arthur, M. A., & Sageman, B. B. (1994). Marine black shales: depositional mechanisms and environments of ancient deposits. *Annual Review of Earth and Planetary Sciences*, 22(1), 499-551.
- Azmy, K., Kendall, B., Brand, U., Stouge, S., & Gordon, G. W. (2015). Redox conditions across the Cambrian–Ordovician boundary: Elemental and isotopic signatures retained in the GSSP carbonates. *Palaeogeography, Palaeoclimatology, Palaeoecology*, 440, 440-454. doi:10.1016/j.palaeo.2015.09.014
- Banjade, B. (2011). *Subsurface Facies Analysis of the Cambrian Conasauga Formation and Kerbel Formation in East-Central Ohio*. Bowling Green State University.
- Bau, M. (1999). Scavenging of dissolved yttrium and rare earths by precipitating iron oxyhydroxide: experimental evidence for Ce oxidation, Y-Ho fractionation, and lanthanide tetrad effect. *Geochimica et Cosmochimica Acta*, 63(1), 67-77.
- Bau, M., & Dulski, P. (1996). Distribution of yttrium and rare-earth elements in the Penge and Kuruman iron-formations, Transvaal Supergroup, South Africa. *Precambrian Research*, 79(1), 37-55. doi:[http://dx.doi.org/10.1016/0301-9268\(95\)00087-9](http://dx.doi.org/10.1016/0301-9268(95)00087-9)

- Berry, W. B., & Wilde, P. (1978). Progressive ventilation of the oceans; an explanation for the distribution of the lower Paleozoic black shales. *American Journal of Science*, 278(3), 257-275.
- Blakey, R. (Producer). (2005, 02/05/2017). Paleogeography and Geologic Evolution of North America. Retrieved from <https://www2.nau.edu/rcb7/namC500.jpg>
- Brasier, M. (1993). Towards a carbon isotope stratigraphy of the Cambrian System: potential of the Great Basin succession. *Geological Society, London, Special Publications*, 70(1), 341-350.
- Brennecka, G. A., Herrmann, A. D., Algeo, T. J., & Anbar, A. D. (2011). Rapid expansion of oceanic anoxia immediately before the end-Permian mass extinction. *Proc Natl Acad Sci U S A*, 108(43), 17631-17634. doi:10.1073/pnas.1106039108
- Brumsack, H.-J. (2006). The trace metal content of recent organic carbon-rich sediments: Implications for Cretaceous black shale formation. *Palaeogeography, Palaeoclimatology, Palaeoecology*, 232(2-4), 344-361. doi:10.1016/j.palaeo.2005.05.011
- Canfield, D. E., & Teske, A. (1996). Late proterozoic rise in atmospheric oxygen concentration inferred from phylogenetic and sulphur-isotope studies. *Nature*, 382(6587), 127.
- Claypool, G. E., & Kaplan, I. (1974). The origin and distribution of methane in marine sediments *Natural gases in marine sediments* (pp. 99-139): Springer.
- Dahl, T. W., Boyle, R. A., Canfield, D. E., Connelly, J. N., Gill, B. C., Lenton, T. M., & Bizzarro, M. (2014). Uranium isotopes distinguish two geochemically distinct stages during the later Cambrian SPICE event. *Earth Planet Sci Lett*, 401, 313-326. doi:10.1016/j.epsl.2014.05.043
- Denison, R. E., Koepnick, R. B., Burke, W. H., & Hetherington, E. A. (1998). Construction of the Cambrian and Ordovician seawater ⁸⁷Sr/⁸⁶Sr curve. *Chemical Geology*, 152(3-4), 325-340. doi:[http://dx.doi.org/10.1016/S0009-2541\(98\)00119-3](http://dx.doi.org/10.1016/S0009-2541(98)00119-3)
- Derry, L. A., Kaufman, A. J., & Jacobsen, S. B. (1992). Sedimentary cycling and environmental change in the Late Proterozoic: evidence from stable and radiogenic isotopes. *Geochimica et Cosmochimica Acta*, 56(3), 1317-1329.
- Dong, D., Nelson, Y. M., Lion, L. W., Shuler, M. L., & Ghiorse, W. C. (2000). Adsorption of Pb and Cd onto metal oxides and organic material in natural surface coatings as determined by selective extractions: new evidence for the importance of Mn and Fe oxides. *Water Research*, 34(2), 427-436.
- Ettensohn, F. R. (2008). Chapter 4 The Appalachian Foreland Basin in Eastern United States. In D. M. Andrew (Ed.), *Sedimentary Basins of the World* (Vol. Volume 5, pp. 105-179): Elsevier.

- Fantle, M. S., & Higgins, J. (2014). The effects of diagenesis and dolomitization on Ca and Mg isotopes in marine platform carbonates: implications for the geochemical cycles of Ca and Mg. *Geochimica et Cosmochimica Acta*, 142, 458-481.
- Gao, D., Shumaker, R. C., & Wilson, T. H. (2000). Along-Axis Segmentation and Growth History of the Rome Trough in the Central Appalachian Basin. *AAPG bulletin*, 84(1), 75-99.
- Gerhardt, A. M., & Gill, B. C. (2016). Elucidating the relationship between the later Cambrian end-Marjuman extinctions and SPICE Event. *Palaeogeography, Palaeoclimatology, Palaeoecology*, 461, 362-373.
- Gill, B. C., Lyons, T. W., Young, S. A., Kump, L. R., Knoll, A. H., & Saltzman, M. R. (2011). Geochemical evidence for widespread euxinia in the later Cambrian ocean. *Nature*, 469(7328), 80-83. doi:10.1038/nature09700
- Glumac, B., & Mutti, L. E. (2007). Late Cambrian (Steptoean) sedimentation and responses to sea-level change along the northeastern Laurentian margin: Insights from carbon isotope stratigraphy. *Geological Society of America Bulletin*, 119(5-6), 623-636. doi:10.1130/b25897.1
- Glumac, B., & Walker, K. R. (1998). A Late Cambrian positive carbon-isotope excursion in the southern Appalachians: Relation to biostratigraphy, sequence stratigraphy, environments of deposition, and diagenesis. *Journal of Sedimentary Research*, 68(6).
- Glumac, B., & Walker, K. R. (2000). Carbonate deposition and sequence stratigraphy of the terminal Cambrian grand cycle in the southern Appalachians, USA. *Journal of Sedimentary Research*, 70(4), 952-963.
- Gromet, L. P., Haskin, L. A., Korotev, R. L., & Dymek, R. F. (1984). The "North American shale composite": its compilation, major and trace element characteristics. *Geochimica et Cosmochimica Acta*, 48(12), 2469-2482.
- Harris, D., Hickman, J., Baranoski, M., Drahovzal, J., Avery, K., & Nuttall, B. (2004). Rome Trough Consortium final report and data distribution: Kentucky Geological Survey, ser. 12. *Open File Report*, 04-06.
- Hasson, K., & Haase, C. S. (1988). Lithofacies and paleogeography of the Conasauga Group, (Middle and Late Cambrian) in the Valley and Ridge province of east Tennessee. *Geological Society of America Bulletin*, 100, 234-246.
- Hasson, K. O., & Haase, C. S. (1988). Lithofacies and paleogeography of the Conasauga Group, (Middle and Late Cambrian) in the Valley and Ridge province of east Tennessee. *Geological Society of America Bulletin*, 100(2), 234-246.
- Hearn, P. P., & Sutter, J. f. (1985a). Authigenic Potassium Feldspar in Cambrian Carbonates: Evidence of Alleghanian Brian Migration. *Science*, 228(4707), 1529-1531.

- Hearn, P. P., & Sutter, J. F. (1985b). Authigenic potassium feldspar in Cambrian carbonates: evidence of Alleghanian brine migration. *Science*, 228(4707), 1529-1531.
- Irwin, H., Curtis, C., & Coleman, M. (1977). Isotopic evidence for source of diagenetic carbonates formed during burial of organic-rich sediments. *Nature*, 269(5625), 209-213.
- Janssens, A. (1973). *Stratigraphy of the Cambrian and Lower Ordovician rocks in Ohio*: State of Ohio, Division of Geological Survey.
- Jonas, L., Müller, T., Dohmen, R., Immenhauser, A., & Putlitz, B. (2017). Hydrothermal replacement of biogenic and abiogenic aragonite by Mg-carbonates—Relation between textural control on effective element fluxes and resulting carbonate phase. *Geochimica et Cosmochimica Acta*, 196, 289-306.
- Jones, B., & Manning, D. A. (1994). Comparison of geochemical indices used for the interpretation of palaeoredox conditions in ancient mudstones. *Chemical Geology*, 111(1-4), 111-129.
- Kouchinsky, A., Bengtson, S., Gallet, Y., Korovnikov, I., Pavlov, V., Runnegar, B., . . . Ziegler, K. (2008). The SPICE carbon isotope excursion in Siberia: a combined study of the upper Middle Cambrian—lowermost Ordovician Kulyumbe River section, northwestern Siberian Platform. *Geological Magazine*, 145(05). doi:10.1017/s0016756808004913
- Kump, L. R., & Arthur, M. A. (1999). Interpreting carbon-isotope excursions: carbonates and organic matter. *Chemical Geology*, 161(1), 181-198.
- Ling, H.-F., Chen, X., Li, D., Wang, D., Shields-Zhou, G. A., & Zhu, M. (2013). Cerium anomaly variations in Ediacaran—earliest Cambrian carbonates from the Yangtze Gorges area, South China: implications for oxygenation of coeval shallow seawater. *Precambrian Research*, 225, 110-127.
- Lyons, T. W., Anbar, A. D., Severmann, S., Scott, C., & Gill, B. C. (2009). Tracking euxinia in the ancient ocean: a multiproxy perspective and Proterozoic case study. *Annual Review of Earth and Planetary Sciences*, 37, 507-534.
- Lyons, T. W., & Severmann, S. (2006). A critical look at iron paleoredox proxies: New insights from modern euxinic marine basins. *Geochimica et Cosmochimica Acta*, 70(23), 5698-5722. doi:<http://dx.doi.org/10.1016/j.gca.2006.08.021>
- Meyer, E. E., Quicksall, A. N., Landis, J. D., Link, P. K., & Bostick, B. C. (2012). Trace and rare earth elemental investigation of a Sturtian cap carbonate, Pocatello, Idaho: Evidence for ocean redox conditions before and during carbonate deposition. *Precambrian Research*, 192-195, 89-106. doi:10.1016/j.precamres.2011.09.015
- Meyer, K. M., & Kump, L. R. (2008). Oceanic Euxinia in Earth History: Causes and Consequences. *Annual Review of Earth and Planetary Sciences*, 36(1), 251-288. doi:10.1146/annurev.earth.36.031207.124256

- Montañez, I. P., Banner, J. L., Osleger, D. A., Borg, L. E., & Bosserman, P. J. (1996). Integrated Sr isotope variations and sea-level history of Middle to Upper Cambrian platform carbonates: Implications for the evolution of Cambrian seawater $^{87}\text{Sr}/^{86}\text{Sr}$. *Geology*, *24*(10), 917-920.
- Ng, T.-W., Yuan, J.-L., & Lin, J.-P. (2014). The North China Steptoean Positive Carbon Isotope Event: New insights towards understanding a global phenomenon. *Geobios*, *47*(6), 371-387. doi:10.1016/j.geobios.2014.09.003
- Nothdurft, L. D., Webb, G. E., & Kamber, B. S. (2004). Rare earth element geochemistry of Late Devonian reefal carbonates, Canning Basin, Western Australia: confirmation of a seawater REE proxy in ancient limestones. *Geochimica et Cosmochimica Acta*, *68*(2), 263-283. doi:10.1016/s0016-7037(03)00422-8
- Osleger, D., & Read, J. F. (1993). Comparative analysis of methods used to define eustatic variations in outcrop: Late Cambrian interbasinal sequence development. *American Journal of Science;(United States)*, *293*(3).
- Ozaki, K., Tajima, S., & Tajika, E. (2011). Conditions required for oceanic anoxia/euxinia: Constraints from a one-dimensional ocean biogeochemical cycle model. *Earth and Planetary Science Letters*, *304*(1-2), 270-279. doi:10.1016/j.epsl.2011.02.011
- Öztürk, M. (1995). Trends of trace metal (Mn, Fe, Co, Ni, Cu, Zn, Cd and Pb) distributions at the oxic-anoxic interface and in sulfidic water of the Drammensfjord. *Marine chemistry*, *48*(3-4), 329-342. doi:[http://dx.doi.org/10.1016/0304-4203\(95\)92785-Q](http://dx.doi.org/10.1016/0304-4203(95)92785-Q)
- Pashin, J. C., Kopaska-Merkel, D. C., Arnold, A. C., McIntyre, M. R., & Thomas, W. A. (2012). Gigantic, gaseous mushwads in Cambrian shale: Conasauga Formation, southern Appalachians, USA. *International Journal of Coal Geology*, *103*, 70-91. doi:10.1016/j.coal.2012.05.010
- Railsback, L. B., Holland, S. M., Hunter, D. M., Jordan, E. M., Díaz, J. R., & Crowe, D. E. (2003). Controls on geochemical expression of subaerial exposure in Ordovician limestones from the Nashville Dome, Tennessee, USA. *Journal of Sedimentary Research*, *73*(5), 790-805.
- Raiswell, R., & Canfield, D. E. (1998). Sources of iron for pyrite formation in marine sediments. *American Journal of Science*, *298*(3), 219-245.
- Read, J. F., & Repetski, J. E. (2012). Cambrian–lower Middle Ordovician passive carbonate margin, southern Appalachians.
- Redfield, A. C. (1958). The biological control of chemical factors in the environment. *American scientist*, *46*(3), 230A-221.
- Ryder, R., Harris, D., Gerome, P., Hainsworth, T., Burruss, R., Lillis, P., . . . Pawlewicz, M. (2005). *Evidence for Cambrian Petroleum Source Rocks in the Rome Trough of West Virginia and Kentucky, Appalachian Basin*. Retrieved from

- Ryder, R. T., Trippi, M. H., Swezey, C. S., Lentz, E. E., Rowan, E. L., & Hope, R. S. *Geologic cross section DD' through the Appalachian Basin from the Findlay Arch, Sandusky County, Ohio, to the Valley and Ridge Province, Hardy County, West Virginia.*
- Saito, M. A., Sigman, D. M., & Morel, F. M. M. (2003). The bioinorganic chemistry of the ancient ocean: the co-evolution of cyanobacterial metal requirements and biogeochemical cycles at the Archean–Proterozoic boundary? *Inorganica Chimica Acta*, 356, 308-318. doi:[http://dx.doi.org/10.1016/S0020-1693\(03\)00442-0](http://dx.doi.org/10.1016/S0020-1693(03)00442-0)
- Saltzman, M., Cowan, C., Runkel, A., Runnegar, B., Stewart, M., & Palmer, A. (2004). The Late Cambrian SPICE (13C) event and the Sau II-Sauk III regression: new evidence from Laurentian Basins in Utah, Iowa, and Newfoundland. *Journal of Sedimentary Research*, 74(3), 366-377.
- Saltzman, M., Ripperdan, R., Brasier, M. D., Lohmann, K., Robinson, R., Chang, w., . . . Runnegar, B. (2000). A global carbon isotope excursion (SPICE) during the Late Cambrian: relation to trilobite extinctions, organic-matter burial and sea level. *Paleogeography, Paleoclimatology, Paleoecology*, 211-223.
- Saltzman, M., & Thomas, E. (2012). Carbon isotope stratigraphy. *The Geologic Time Scale*, 1, 207-232.
- Saltzman, M. R. (2005). Phosphorus, nitrogen, and the redox evolution of the Paleozoic oceans. *Geology*, 33(7), 573. doi:10.1130/g21535.1
- Saltzman, M. R., Davidson, J. P., Holden, P., Runnegar, B., & Lohmann, K. C. (1995). Sea-level-driven changes in ocean chemistry at an Upper Cambrian extinction horizon. *Geology*, 23(10), 893-896.
- Saltzman, M. R., Ripperdan, R. L., Brasier, M., Lohmann, K. C., Robison, R. A., Chang, W., . . . Runnegar, B. (2000). A global carbon isotope excursion (SPICE) during the Late Cambrian: relation to trilobite extinctions, organic-matter burial and sea level. *Palaeogeography, Palaeoclimatology, Palaeoecology*, 162(3), 211-223.
- Saltzman, M. R., Runnegar, B., & Lohmann, K. C. (1998). Carbon isotope stratigraphy of Upper Cambrian (Stephanian Stage) sequences of the eastern Great Basin: Record of a global oceanographic event. *Geological Society of America Bulletin*, 110(3), 285-297.
- Saltzman, M. R., Young, S. A., Kump, L. R., Gill, B. C., Lyons, T. W., & Runnegar, B. (2011). Pulse of atmospheric oxygen during the late Cambrian. *Proc Natl Acad Sci U S A*, 108(10), 3876-3881. doi:10.1073/pnas.1011836108
- Schippers, A., & Jørgensen, B. (2001). Oxidation of pyrite and iron sulfide by manganese dioxide in marine sediments. *Geochimica et Cosmochimica Acta*, 65(6), 915-922.
- Schröder, S., & Grotzinger, J. (2007). Evidence for anoxia at the Ediacaran–Cambrian boundary: the record of redox-sensitive trace elements and rare earth elements in Oman. *Journal of the Geological Society*, 164(1), 175-187.

- Scotese, C.R., 2014. Atlas of Cambrian and Early Ordovician Paleogeographic Maps (Mollweide Projection), Maps 81-88, Volumes 5, The Early Paleozoic, PALEOMAP Atlas for ArcGIS, PALEOMAP Project, Evanston, IL
- Shields, G. A., & Webb, G. E. (2004). Has the REE composition of seawater changed over geological time? *Chemical Geology*, 204(1-2), 103-107. doi:10.1016/j.chemgeo.2003.09.010
- Środoń, J., Drits, V. A., McCarty, D. K., Hsieh, J. C., & Eberl, D. D. (2001). Quantitative X-ray diffraction analysis of clay-bearing rocks from random preparations. *Clays and Clay Minerals*, 49(6), 514-528.
- Taylor, J. F., Repetski, J. E., Loch, J. D., & Leslie, S. A. (2012). Biostratigraphy and chronostratigraphy of the Cambrian–Ordovician great American carbonate bank.
- Taylor, S. R., & McLennan, S. M. (1985). The continental crust: its composition and evolution.
- Thomas, W. (1991). The Appalachian-Ouchita rifted margin of southeastern North America. *Geological Society of America Bulletin*, 415-431.
- Tissot, F., & Dauphas, N. (2015). Uranium isotopic compositions of the crust and ocean: Age corrections, U budget and global extent of modern anoxia. *Geochimica et Cosmochimica Acta*, 113-143.
- Tostevin, R., Shields, G. A., Tarbuck, G. M., He, T., Clarkson, M. O., & Wood, R. A. (2016). Effective use of cerium anomalies as a redox proxy in carbonate-dominated marine settings. *Chemical Geology*, 438, 146-162. doi:<http://dx.doi.org/10.1016/j.chemgeo.2016.06.027>
- Tribouvillard, N., Algeo, T. J., Lyons, T., & Riboulleau, A. (2006). Trace metals as paleoredox and paleoproductivity proxies: an update. *Chemical Geology*, 232(1), 12-32.
- Wall, A. J., Capo, R. C., Stewart, B. W., Phan, T. T., Jain, J. C., Hakala, J. A., & Guthrie, G. D. (2013). High throughput method for Sr extraction from variable matrix waters and ⁸⁷Sr/⁸⁶Sr isotope analysis by MC-ICP-MS. *Journal of Analytical Atomic Spectrometry*, 28(8), 1338-1344.
- Webb, G. E., & Kamber, B. S. (2000). Rare earth elements in Holocene reefal microbialites: a new shallow seawater proxy. *Geochimica et Cosmochimica Acta*, 64(9), 1557-1565.
- Wignall, P. B., & Twitchett, R. J. (1996). Oceanic anoxia and the end Permian mass extinction. *Science*, 272(5265), 1155.
- Woods, M. A., Wilby, P. R., Leng, M. J., Rushton, A. W. A., & Williams, M. (2011). The Furongian (late Cambrian) Steptoean Positive Carbon Isotope Excursion (SPICE) in Avalonia. *Journal of the Geological Society*, 168(4), 851-862. doi:10.1144/0016-76492010-111

Zhang, K., Zhu, X.-K., & Yan, B. (2015). A refined dissolution method for rare earth element studies of bulk carbonate rocks. *Chemical Geology*, 412, 82-91.
doi:10.1016/j.chemgeo.2015.07.027